THE GEOLOGICAL SOCIETY OF AMERICA®

Regional exhumation of the Laramide Province

Gilby Jepson[1,2,†], Barbara Carrapa[2], Lauren J. Reeher[2,3], Peter G. DeCelles[2], Walter D. Afonso[2], Caden J. Howlett[2], Emilia A. Caylor[2], Tshering Z.L. Sherpa[2], Jordan W. Wang[2], and Kurt N. Constenius[2]

[1]*School of Geosciences, University of Oklahoma, Norman, Oklahoma 73019, USA*
[2]*Department of Geosciences, University of Arizona, Tucson, Arizona 85721, USA*
[3]*Utah Geological Survey, Salt Lake City, Utah 84116, USA*

ABSTRACT

Western North America is the archetypical Cordilleran orogenic system that preserves a Mesozoic to Cenozoic record of oceanic Farallon plate subduction-related processes. After prolonged Late Jurassic through mid-Cretaceous normal-angle Farallon plate subduction that produced the western North American batholith belt and retroarc fold-thrust belt, a period of low-angle, flat-slab subduction during Late Cretaceous–Paleogene time caused upper plate deformation to migrate eastward in the form of the Laramide basement-involved uplifts, which partitioned the original regional foreland basin. Major questions persist about the mechanism and timing of flat-slab subduction, the trajectory of the flat-slab, inter-plate coupling mechanism(s), and the upper-plate deformational response to such processes. Critical for testing various flat-slab hypotheses are the timing, rate, and distribution of exhumation experienced by the Laramide uplifts as recorded by low-temperature thermochronology. In this contribution, we address the timing of regional exhumation of the Laramide uplifts by combining apatite fission-track (AFT) and (U-Th-Sm)/He (AHe) data from 29 new samples with 564 previously published AFT, AHe, and zircon (U-Th)/He ages from Laramide structures in Arizona, Utah, Wyoming, Colorado, Montana, and South Dakota, USA. We integrate our results with existing geological constraints and with new regional cross sections to reconstruct the spatial and temporal history of exhumation driven by Laramide deformation from the mid-Cretaceous to Paleogene. Our analysis suggests a two-stage exhumation of the Laramide province, with an early phase of localized exhumation occurring at ca. 100–80 Ma in Wyoming and Montana, followed by a more regional period of exhumation at ca. 70–50 Ma. Generally, the onset of enhanced exhumation occurs earlier in the northern Laramide province (ca. 90 Ma) and later in the southern Laramide province (ca. 80 Ma). Thermal history models of selected samples along regional cross sections through Utah–Arizona–New Mexico and Wyoming–South Dakota show that exhumation occurred contemporaneously with deformation, implying that Laramide basement block exhumation is coupled with regional deformation. These results have implications for testing proposed migration pathway models of Farallon flat-slab and for how upper-plate deformation is expressed in flat-slab subduction zones in general.

INTRODUCTION

The North American Cordillera is a well-preserved example of an orogenic system involving a subducting oceanic plate and overriding continental plate (e.g., Burchfiel and Davis, 1972; DeCelles, 2004; Yonkee and Weil, 2015; Lawton, 2019). Subduction of the oceanic Farallon plate initiated as early as ca. 180 Ma (Mulcahy et al., 2018) but did not become strongly coupled to the overriding North American plate until the Late Jurassic (ca. 155 Ma) following regional accretion of parautochthonous arc terranes and closure of marginal ocean basins (Harper and Wright, 1984; Wright and Fahan, 1988; Saleeby, 1992; Saleeby and Busby-Spera, 1992; Dickinson et al., 1996). The transition to a simple, two-plate, east-dipping ocean-continent subduction system at the latitudes of California, USA, occurred at ca. 155 Ma and marked the onset of growth of the Cordilleran orogenic belt, which is thought to have two major shortening "events," referred to as the Sevier (Armstrong, 1968) and Laramide orogenies (e.g., Blackwelder, 1914; Brown, 1988). The difference between these two events is generally a matter of tectonic style and spatial distribution, with the Sevier having mainly a thin-skinned thrust belt style and the Laramide being a thick-skinned basement-involved style. The Sevier and Laramide structures are also spatially separate (with only very local spatial overlap): the Sevier belt is characterized by a linear group of closely spaced thrust faults and related folds (from Las Vegas, Nevada, USA, to the Idaho state line, USA) concentrated along the frontal portion of the much larger Cordilleran belt (e.g., Allmendinger, 1992; DeCelles, 2004), which extends latitudinally from Sonora, Mexico, to the Yukon Territory, Canada, and eastward from Nevada to western Wyoming, USA, following the former passive margin of western North America (Fig. 1). The Laramide uplifts, however, are restricted to the western interior region of Montana, Wyoming, Utah, Colorado, Arizona, New Mexico, and South Dakota, USA. The Cordilleran orogen involved a magmatic arc, crustal thickening, and surface uplift (e.g., Livaccari, 1991; Lawton et al., 1994; Bahadori et al., 2022). A regional foreland basin developed east of the frontal Sevier belt in response to flexural loading and subsidence from Late Jurassic to Late Cretaceous time (e.g., Jordan, 1981; Cross, 1986; Kauffman and Caldwell, 1993; DeCelles, 2004; Miall et al., 2008). The regional subsidence pattern transitioned from mostly flexural to flexural plus dynamic subsidence beginning ca. 81 Ma associated with shallowing of the subducting plate (e.g., Mitrovica et al., 1989; Pang and Nummedal, 1995; Painter and Carrapa, 2013). Beginning in the Late Cretaceous, the foreland basin was partitioned by basement-involved uplifts and associated intervening intraforeland basins (e.g., Saylor et al., 2020; Erslev et al., 2022; Weil and Yonkee, 2023). Most of the uplifts are bounded by variably dipping reverse faults that extend downward to mid-crustal depths (e.g., Smithson et al., 1978). These intraforeland basement uplifts and basins define the "Laramide province" (Brown, 1988; Weil and Yonkee, 2023). Thin-skinned shortening in

Gilby Jepson https://orcid.org/0000-0003-0151-3062
[†]gjepson@ou.edu

GSA Bulletin;
published online 18 February 2025

https://doi.org/10.1130/B37625.1.

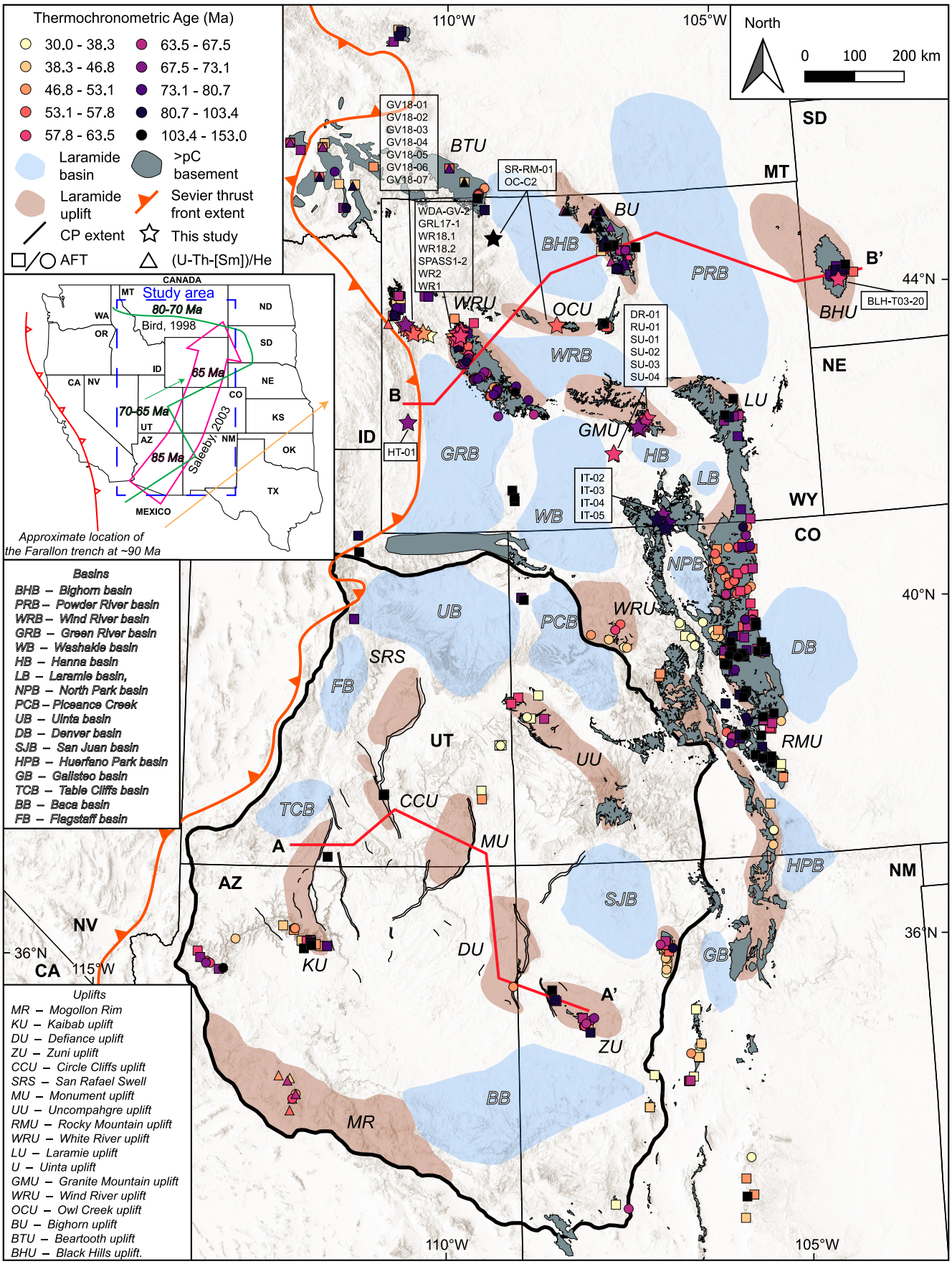

Figure 1. Map of the Laramide province (including the Colorado Plateau [CP]), western United States, showing locations of low-temperature thermochronometric data (apatite fission-track [AFT], apatite [U-Th-Sm]/He, and zircon [U-Th]/He) between 153 Ma and 30 Ma. Circles denote published AFT samples with a mean track length (MTL) >13 µm, indicative of relatively rapid cooling. Squares denote samples that have either MTLs <13 µm or no MTLs reported, indicative of relatively low cooling or more complex cooling histories. Triangles denote apatite and zircon (U-Th-[Sm])/He ages and stars denote samples from this study. Orange arrow represents Farallon-Pacific plate convergence direction after Torsvik et al. (2019). Cross-section trace is denoted by red lines, with A to A′ shown in Figure 2 and B to B′ shown in Figure 3. AZ—Arizona; CA—California; CO—Colorado; ID—Idaho; KS—Kansas; MT—Montana; ND—North Dakota; NE—Nebraska; NM—New Mexico; NV—Nevada; OK—Oklahoma; OR—Oregon; SD—South Dakota; TX—Texas; UT—Utah; WA—Washington; WY—Wyoming.

the Sevier fold-thrust belt continued through the early Eocene overlapping temporally with Laramide deformation (DeCelles, 2004). The onset of Laramide basement-involved uplifts, in conjunction with the shutdown of the Sierra Nevada arc segment at ca. 80 Ma (Cecil et al., 2012), shutdown of the Mojave arc sector at ca. 70 Ma (Schwartz et al., 2023), and inboard migration of igneous activity to the Colorado Mineral Belt (Chapin, 2012), are interpreted to be the product of shallowing of the Farallon slab and subsequent flat-slab subduction (e.g., Dickinson and Snyder, 1978; Livaccari et al., 1981; Axen et al., 2018).

The Laramide orogenic event is of geodynamic relevance because it preserves a record of Cordilleran processes that serve as an ancient counterpart for modern and paleo flat-slab subduction systems and far-field intracontinental deformation (Jordan and Allmendinger, 1986; Zuza et al., 2018; Clinkscales and Kapp, 2019; Tan et al., 2022; George et al., 2022). Two broad categories of models have been proposed to explain how deformation is transmitted from the subducting flat slab to the overriding plate. The first category, basal traction, associates deformation with increased shear coupling during subduction, with a relatively short stress transmission distance between the upper crust and a low-angle slab (e.g., Bird, 1984, 1998; Copeland et al., 2017; Weil and Yonkee, 2023). The second category, end-loading, associates deformation with the occurrence of an end-load on the overriding plate, which causes a regionally extensive compressional stress state (e.g., Oldow et al., 1989; Livaccari, 1991; Axen et al., 2018; Erslev et al., 2022).

Within the basal-shear mechanism for deformation, the distribution and timing of exhumation of Laramide structures can be used as a proxy for the timing and location of flat slab subduction (e.g., Bird, 1998; Copeland et al., 2017). There are two favored groups of models for the trajectory of the Farallon flat slab. The first set hypothesize that slab flattening initiated at ca. 90–80 Ma and migrated from the south-southwest (present-day Mojave region) to the north-northeast along a narrow corridor (e.g., Saleeby, 2003; Liu et al., 2010; Copeland et al., 2017). These models rely on subduction of an oceanic plateau or aseismic ridge (Shatsky and Hess rise conjugates; e.g., Livaccari et al., 1981; Henderson et al., 1984; Saleeby, 2003; Liu et al., 2010). However, shapes and existence of Shatsky-Hess conjugates remain uncertain (Torsvik et al., 2019; Sano et al., 2020). The second set hypothesize an uneven plate geometry and initiation of flat-slab subduction at ca. 80 Ma beneath much of the California margin, which later migrated east into the western interior (e.g., Bird, 1984). This second group of models does not require plateau or ridge subduction and instead invokes a combination of upper and lower plate processes, such as increased convergence rate (Engebretson et al., 1984), transmission of shear stresses inboard (Dickinson and Snyder, 1978; Bird, 1984, 1998), and/or upward forces derived from asthenospheric flow near the deep keel of the Wyoming cratonic lithosphere (Jones et al., 2011). Because the broad, uneven plate geometry does not involve spatially limited features on the subducting Farallon plate, it can better explain the broad spatial distribution of Laramide deformation, the temporal overlap in thin-skinned and thick-skinned deformation, and the diachroneity of exhumation, and it permits more variable slab trajectories.

One way to assess various models for the Laramide orogenic event is to establish the regional pattern of exhumation of Laramide uplifts using low-temperature thermochronology. Low-temperature thermochronology records the time at which a rock passes through a given temperature window or closure temperature (T_c) and can be used as a proxy for cooling and exhumation (e.g., Reiners and Brandon, 2006; Braun et al., 2006). As a result, low-temperature thermochronology, more specifically apatite fission-track (AFT, partial annealing zone = 120–60 °C), apatite (U-Th-Sm)/He (AHe, T_c = 80–40 °C), and zircon (U-Th)/He (ZHe, T_c = 200–150 °C), has long been used to date exhumation of Laramide uplifts (e.g., Cerveny and Steidtmann, 1993; Omar et al., 1994; Kelley et al., 1992, 2001; Kelley, 2005; Naeser et al., 2002; Peyton et al., 2012; Kelley and Karlstrom, 2012; Peyton and Carrapa, 2013; Stevens et al., 2016; Winn et al., 2017; Rønnevik et al., 2017; Carrapa et al., 2019; Thacker et al., 2021; Davis et al., 2022; Caylor et al., 2023; Howlett et al., 2024). Currently, the body of published Laramide thermochronometric data, when combined with structural data, is sufficient to address the following questions: (1) Is the timing of exhumation of Laramide uplifts compatible with the location of the flattened Farallon slab? (2) If so, does the distribution of thermochronometric ages favor a particular trajectory/model? (3) Did stress driving deformation propagate into the North American craton as a function of basal-shear or end-loading? In this contribution, we aim to address these questions by integrating new AFT and AHe data from 29 samples from multiple Laramide uplifts across Wyoming, South Dakota, and Colorado, along with 564 previously published thermochronometric ages (AFT, AHe, and ZHe). We consider these data within the context of regional structural cross sections and thermal history modeling from selected Laramide uplifts to evaluate the regional spatial and temporal distribution of Laramide exhumation.

TECTONIC BACKGROUND

The North American Cordillera has long been interpreted as the product of subduction of the oceanic Farallon plate beneath continental North America beginning during the Late Jurassic (ca. 160 Ma) when the convergent margin became a simple two-plate system (Hamilton, 1969; Oldow et al., 1989; Burchfiel et al., 1992; Smith et al., 1993; Dickinson et al., 1996; DeCelles, 2004; Weil and Yonkee, 2012). The paleo-Farallon trench strikes N-S to NW-SE along the western margin of continental North America with convergence occurring obliquely to the plate boundary (e.g., Engebretson et al., 1984; Saleeby et al., 1992). During Late Jurassic to mid-Cretaceous time, convergence velocity between the Farallon and North American plates increased from $\leq$5 cm/yr to $\geq$10 cm/yr (Engebretson et al., 1984; DeCelles, 2004; Doubrovine and Tarduno, 2008; Yonkee and Weil, 2015; Liu and Currie, 2016). Subduction of the Farallon plate formed an extensive continental magmatic arc extending from the Yukon to Baja California

(Fig. 1) largely composed of calc-alkaline granitoid rocks (Ducea and Barton, 2007; Gehrels et al., 2009; Cecil et al., 2012; Schwartz et al., 2021). In the Sierra Nevada batholith, the magmatic arc exhibits two main phases of voluminous magma production: one during the Late Jurassic (160–150 Ma) and a second during the mid- to Late Cretaceous (100–85 Ma; Ducea and Saleeby, 1998; Ducea, 2001).

Retroarc shortening during growth of the Cordillera was accommodated by folding and thrusting of Neoproterozoic–Jurassic passive margin and platformal sedimentary rocks from the eastern flank of the Sierra Nevada to Nevada, central Utah, Idaho, and western Montana and Wyoming (e.g., Dunne and Walker, 1993; Carpenter et al., 1993; Mitra, 1997; Taylor et al., 2000; Currie, 2002; Wyld, 2002; DeCelles, 2004; DeCelles and Coogan, 2006; Greene, 2014; Long, 2012, 2015; Long et al., 2014; Yonkee and Weil, 2015; Giallorenzo et al., 2018; Yonkee et al., 2019). The eastern part of the Cordilleran thrust belt in central Utah, western Wyoming, and eastern Idaho is referred to as the Sevier belt (Armstrong, 1968). Although much of the Cordilleran deformation is known from surface exposures of upper crustal level structures, particularly in the frontal Sevier belt, its mid-crustal ductile expression, as well as voluminous partial melting, is locally well documented (e.g., Snoke and Miller, 1988; Miller et al., 1988; Miller and Gans, 1989; Camilleriand Chamberlain, 1997; McGrew et al., 2000; Wells and Hoisch, 2008). Anatectic melts formed ca. 95–65 Ma in Nevada and northern Utah and ca. 85–40 Ma in southern Arizona and northern Sonora (Miller and Bradfish, 1980; Chapman et al., 2021). Partial melting is correlated with the Cretaceous–Eocene emplacement of peraluminous muscovite-bearing granites associated with anatexis and has been associated with decoupling of the crust-mantle boundary (Vlaha et al., 2024). Shortening in the Cordilleran fold-thrust belt commenced during late Middle Jurassic time and continued through the early Eocene in the frontal Sevier belt (ca. 50 Ma, e.g., DeCelles, 2004; Giallorenzo et al., 2018; Yonkee et al., 2019). Major thrust faults propagated eastward through time and generally climbed stratigraphically upward from Neoproterozoic strata in the basal western part of the belt to Cretaceous strata, with local basement involvement (Royse et al., 1975; DeCelles, 2004; Yonkee and Weil, 2015; Di Fiori et al., 2021; Chapman et al., 2024). A regional foreland basin developed contemporaneously and in response to the eastward migrating Cordilleran fold-thrust belt.

During the Late Cretaceous–Paleocene, thick-skinned deformation began to occur within the foreland basin, east of the frontal Sevier fold-thrust belt. Unlike most of the deformation in the fold-thrust belt, the intraforeland deformation mainly involved Archean–Proterozoic crystalline basement, which was overlain by a relatively thin (~1.5–3 km) Paleozoic–Mesozoic stratigraphic section. The change in deformational style occurred along with a Late Cretaceous change from flexural to flexural and dynamic basin subsidence (e.g., Pang and Nummedal, 1995; Painter and Carrapa, 2013; Heller and Liu, 2016). This change to basement-involved faulting and more dynamic subsidence has been correlated with similar observations in the South American Cordillera latitudes in which the subducting slab becomes subhorizontal (e.g., Jordan and Allmendinger, 1986). Major Laramide uplifts, some of which reactivated preexisting basement shear zones and Ancestral Rocky Mountains faults, formed a complex of anastomosing basement uplifts and intervening flexural basins (e.g., Keefer, 1970; Schmidt and Garihan, 1983; Dickinson et al., 1988; Erslev, 1993; Neely and Erslev, 2009; Weil et al., 2016; Lawton, 2019). Shortening in the fold-thrust belt continued while Laramide structures partitioned the foreland region into a broken foreland setting (Jordan, 1981; Constenius et al., 2003; DeCelles, 2004). Laramide deformation at latitudes 36°–42°N coincided with a period of progressive shutdown of the Sierra Nevada (ca. 80 Ma) and Mojave arc (ca. 70 Ma) segments, an eastward magmatic sweep, and the transition from mostly flexural to dynamic basin subsidence (e.g., Coney and Reynolds, 1977; Bird, 1984; Cross, 1986; Mitrovica et al., 1989; Dumitru, 1990; Constenius et al., 2003; Liu et al., 2011; Paterson et al., 2011; Cecil et al., 2012; Painter and Carrapa, 2013; Premo et al., 2014; Economos et al., 2021; Schwartz et al., 2023). The progressive shut-off of the arc combined with eastward underplating of subduction zone rocks led workers to suggest that the Farallon slab had begun shallowing regionally (e.g., Coney and Reynolds, 1977; Bird, 1984; Saleeby, 2003; Constenius et al., 2003; Jacobson et al., 2011). Lower crustal xenolith samples from beneath the Colorado Plateau display eclogite recrystallization and zircon growth between ca. 80 Ma and 33 Ma. Eclogite recrystallization is correlated with the introduction of water associated with flattening of the Farallon slab (e.g., Usui et al., 2003; Smith et al., 2004). Two major mechanisms have been proposed to cause flattening of the Farallon slab: (1) the subduction of buoyant oceanic lithosphere of the conjugates of the Hess and Shatsky Rises (Livaccari et al., 1981; Tarduno et al., 1985) and (2) changes in relative motions of the North American and Farallon plates (e.g., Engebretson et al., 1985; Bird, 1998; Jones et al., 2011). However, the Cretaceous–Paleogene motion of the flattened Farallon slab remains debated, with two contrasting trajectories: an oblique approximately SSW to NNE trajectory (Fig. 1; e.g., Saleeby, 2003; Doubrovine and Tarduno, 2008; Liu et al., 2010; Liu and Currie, 2016; Axen et al., 2018) or an approximately WSW to ENE trajectory as originally proposed by Bird (1998), which allows for flat-slab subduction to initiate earlier to the north as a function of plate paleogeography (Fig. 1; e.g., Carrapa et al., 2019).

By Eocene time, the Farallon slab began to founder and roll back to the west, as evinced by a regional flare-up in silicic back-arc magmatism and west-southwestward retreat of the magmatic front back toward the trench (e.g., Coney and Reynolds, 1977; Feeley, 2003; Constenius et al., 2003; Best et al., 2016; Copeland et al., 2017). Rollback of the Farallon slab led to the gravitational collapse of high topography (~3000 m) by the Paleogene, formation of extensional basins, and exhumation of metamorphic core complexes from Alberta to southern Arizona (e.g., Wells and Hoisch, 2008; Cassel et al., 2018; Howlett et al., 2021; Jepson et al., 2022; Zuza and Cao, 2022; Flansburg and Stockli, 2023; Davis et al., 2023; Zuza et al., 2025). Much of the Oligocene–Miocene and younger extension was concentrated west of the Sevier thrust front. However, Late Cretaceous to Eocene shortening structures and associated intraforeland basins are preserved in the southern Arizona Basin and Range province (e.g., Davis, 1979; Favorito and Seedorff, 2018; Caylor et al., 2021).

METHODS

To decipher the spatio-temporal path of Late Cretaceous–Paleogene cooling and exhumation across the western United States, we compiled 564 published apatite fission-track and apatite (U-Th-Sm)/He ages from prominent Laramide uplifts in Montana, Wyoming, Utah, Colorado, Arizona, New Mexico, and South Dakota (Table S1 in the Supplemental Material[1]; Bryant and Naeser, 1980; Kelley and Duncan, 1986; Cerveny, 1990; Kelley et al., 1992, 2001; Naeser, 1992; Cerveny and Steidtmann, 1993; Roberts and Burbank, 1993; Dumitru et al., 1994; Omar et al., 1994; Strecker, 1996; Kelley and Chapin, 1997; Crowley et al., 2002; Naeser et al., 2002; Kelley and Chapin, 2004; Peyton et al., 2012;

[1]Supplemental Material. Single-grain apatite fission-track data of samples collected in this study; thermal history models, assumptions, and model fits; published low-temperature thermochronological data from the Laramide Province; and a version of Figure 5 filtered for apatite fission-track data with long confined track lengths (>13 μm). Please visit https://doi.org/10.1130/GSAB.S.28220111 to access the supplemental material; contact editing@geosociety.org with any questions.

TABLE 1. NEW SAMPLES COLLECTED FROM LARAMIDE STRUCTURES ACROSS THE WESTERN USA

Sample	Method	Lithology	Age	Latitude (°N)	Longitude (°W)	Elevation (m asl)
IT-02	AFT	Gneiss	Archean	41.0903	106.664	2860
IT-03	AFT	Granite	Proterozoic	40.9827	106.536	2556
IT-04	AFT	Granite	Proterozoic	41.0201	106.516	2605
IT-05	AFT	Gneiss	Archean	41.1319	106.58	2484
DR-01	AFT	Granite	Archean	42.3057	106.782	2051
RU-01	AFT	Sandstone	Cambrian	41.8803	107.329	2286
SU-01	AFT	Gneiss	Archean	42.1525	106.916	2079
SU-02	AFT	Granite	Archean	42.1598	106.909	1879
SU-03	AFT	Granite	Archean	42.1756	106.933	2282
SU-05	AFT	Granite	Archean	42.2325	106.823	1889
HT-01	AFT	Quartzite	Proterozoic	42.3199	110.495	2277
BLH-T03-20	AFT	Granite	Proterozoic	43.7991	103.499	1607
MR20-2	AFT	Granite	Proterozoic	43.8781	103.458	1611
SR-RM-01	AFT	Granite	Archean	44.5017	109.186	1656
OC-C2	AFT	Granite	Archean	43.4497	108.169	1409
GV18-01	AFT/AHe	Granite	Archean	43.5043	110.667	2220
GV18-02	AFT/AHe	Granite	Archean	43.4582	110.629	3162
GV18-03	AFT/AHe	Granite	Archean	43.431	110.589	3013
GV18-04	AFT/AHe	Granite	Archean	43.4192	110.567	2894
GV18-05	AFT/AHe	Granite	Archean	43.377	110.536	2723
GV18-06	AFT/AHe	Granite	Archean	43.3867	110.389	3174
GV18-07	AHe	Granite	Archean	43.341	110.309	2847
WDA-GV-2	AFT	Granite	Archean	43.2898	109.825	2593
GRL17-1	AFT	Granite	Archean	43.1956	109.908	2964
WR18.1	AFT	Granite	Archean	42.7372	109.206	2981
WR18.2	AFT	Granite	Archean	42.4411	108.869	2543
SPASS1-2	AFT	Granite	Archean	43.2989	109.792	2765
WR2	AFT	Granite	Archean	43.2982	109.791	2835
WR1	AFT	Granite	Archean	43.2899	109.825	2593

Note: Age is the reported crystallization age of the rock. AFT—apatite fission-track; AHe—apatite (U-Th-Sm)/He; m asl—meters above sea level.

Painter et al., 2014; Stevens et al., 2016; Brown et al., 2017; Rønnevik et al., 2017; Winn et al., 2017; Carrapa et al., 2019; Murray et al., 2019; Jepson et al., 2021; Thacker et al., 2021; Davis et al., 2022; Caylor et al., 2023; Kapp et al., 2023; Howlett et al., 2024). Despite widespread coverage of low-temperature thermochronology, there remains a paucity of data along smaller, less prominent uplifts. To fill this gap, we collected 29 samples from Laramide uplifts in Colorado, Wyoming, and South Dakota (Table 1; star-symbols, Fig. 1).

Apatite Fission-Track

Apatite fission-track (AFT) thermochronometry relies on the spontaneous fission decay of ^{238}U (Hurford and Green, 1983). Spontaneous fission within apatite creates linear damage zones (tracks) that undergo temperature-dependent shortening in the apatite partial annealing zone at ~120–60 °C (e.g., Wagner and Van den Haute, 1992, and references within). Thus, the statistical relationship among the density of fission tracks, the distribution of confined track lengths, etch pits (D_{par}), composition, and temperature make the AFT system useful for constraining cooling through the upper-crust (e.g., Laslett et al., 1987; Galbraith, 2005; Tamer and Ketcham, 2020). Apatite crystals were mounted in epoxy and polished to reveal their internal section and etched using 5.5 M nitric acid for 20 s at 21 °C before irradiation (after Donelick et al., 2005). Samples were analyzed via the external detector method (Gleadow et al., 1976), which utilizes low uranium muscovite mica detectors that were irradiated together with samples and associated standards at the Oregon State University Triga Reactor, Corvallis, Oregon, USA. The total neutron fluence was determined using CN5 U-doped glass (Bellemans et al., 1995). Following irradiation, the mica sheets were etched in 40% hydrofluoric acid for 45 min at 21 °C (after Carlson et al., 1999; Donelick et al., 2005). Fission-tracks were counted and measured using an Olympus BX51 microscope with an associated digitizing tablet and computer-controlled stage (Kinetek). The fission-track analyses were performed at the University of Arizona Fission Track Laboratory, Tucson, Arizona, USA (Tables 2 and S2). Confined fission-track length distributions and D_{par} were obtained to model cooling histories (Ketcham et al., 2007). The AFT central ages were calculated from single-grain ages determined using the ζ-method after Hurford and Green (1983; see also Table 2).

Apatite (U-Th-Sm)/He

(U-Th-Sm)/He thermochronometry relies on the accumulation and thermally activated diffusion of radiogenic ^{4}He. The apatite partial retention zone for (U-Th-Sm)/He is typically between ~80 °C and 40 °C, making it valuable for determining upper-crustal cooling (e.g., Farley, 2002; Flowers and Kelley, 2011). Apatite (U-Th-Sm)/He (AHe) analyses were performed at the Arizona Radiogenic Helium Dating Laboratory at the University of Arizona and followed the protocols described in Reiners (2005). Helium (^{4}He) was extracted at 900–1300 °C, under ultra-high vacuum with a diode laser, spiked with ^{3}He and measured by quadrupole mass spectrometry following Reiners (2005). Following ^{4}He extraction, tubes that contained degassed apatites were retrieved from the laser cell, dissolved, and analyzed for U and Th isotopes via isotope dilution after addition of ^{233}U-^{229}Th spike on a Thermo Fisher E2 inductively coupled plasma–mass spectrometer (ICP-MS; Reiners, 2005). Blank, sample, as well as spiked standard solutions were subsequently analyzed via isotope dilution for ^{238}U and ^{232}Th, and then with an external calibration for ^{147}Sm via ICP-MS (Reiners, 2005). Replicate analyses of Durango apatite were performed as an internal standard ($n = 4$) yielded a mean (U-Th-Sm)/He age of 30.1 ± 0.4 Ma (1σ), consistent with the Durango (U-Th-Sm)/He reference age of 31.02 ± 1.01 Ma (McDowell et al., 2005).

Thermal History Modeling

Thermal history modeling was performed utilizing AHe and AFT single-grain ages, and associated mean track length (MTL) distributions, with D_{par}. Here, we used the QTQt software (version 5.7.0) to model the thermal history of the samples. The QTQt software applies a Bayesian trans-dimensional approach to Markov Chain Monte Carlo statistics (Gallagher, 2012) to produce a cooling evolution of the sample that predicts the measured data by applying the AFT annealing model after Ketcham et al. (2007) and the AHe diffusion model after Flowers et al. (2009). Models were initiated at temperatures within the apatite partial annealing zone (80 ± 40 °C) at an initial age equal to at least double the measured AFT central age to allow for both full and partial annealing. In our approach, we use an initial unconstrained run to explore the statistical space that was then followed by adjustments to the search parameters as well as the addition of geological constraints. A large number of iterations (>>100,000) were run to generate a range of models that can constrain a probability distribution. From the obtained probability distribution an individual thermal history can be selected, such as the maximum likelihood as well as "expected" (weighted mean) paths. Detailed modeling approach and metadata are available in Figs. S1 and S2 and Table S3 (see Flowers et al., 2015).

Regional Cross Sections

Regional cross sections in Figures 2 and 3 were constructed in Petroleum Experts (Petex) 2D/3D Move software suite using standard techniques. Cross sections were constrained by stratigraphic

TABLE 2. APATITE FISSION-TRACK DATA FROM LARAMIDE UPLIFTS IN COLORADO, WYOMING, AND SOUTH DAKOTA (USA)

Sample	*n**	$\rho_s \times 10^5$ cm^{-2}†	$\rho_D \times 10^5$ cm^{-2}§	$\rho_i \times 10^5$ cm^{-2}#	U ±1σ**	D_{par}††	χ^2§§	Age ±1σ (Ma)	MTL (μm) ± 1σ†††	*n*§§§
Northern Colorado—Southern Wyoming										
IT-02	20	7.0	14.4	19.0	16.2 ± 10.2	2.6	0.31	88.9 ± 7.4##	13.3 ± 1.4	7
IT-03	20	9.9	14.2	28.8	24.8 ± 8.3	2.6	0.53	83.1 ± 5.0##	—	—
IT-04	20	8.6	14.0	27.5	24.0 ± 12.3	2.7	0.65	74.8 ± 3.9##	14.2 ± 0.8	13
IT-05	20	5.7	13.8	19.1	16.9 ± 8.0	2.5	0.90	70.2 ± 4.4##	13.7 ± 1.1	80
DR-01	20	3.4	12.5	11.7	11.5 ± 5.5	3.1	0.99	62.5 ± 4.7##	13.6 ± 1.2	100
RU-01	20	8.0	12.9	29.5	28.0 ± 16.6	2.6	0.31	58.9 ± 4.5##	13.9 ± 1.3	66
SU-01	20	5.3	12.1	16.1	16.2 ± 9.6	2.6	0.81	67.9 ± 4.3##	14.2 ± 0.5	11
SU-02	20	4.4	11.9	13.9	14.2 ± 8.6	2.8	0.89	64.4 ± 4.4##	—	—
SU-03	20	11.6	11.7	31.5	32.7 ± 10.0	2.6	0.95	71.6 ± 3.6##	14.3 ± 1.0	31
SU-05	20	7.9	11.5	24.0	25.4 ± 10.5	2.6	0.95	64.8 ± 3.5##	14.4 ± 0.9	14
Northern Wyoming—South Dakota										
HT-01	20	8.1	12.7	25.1	24.1 ± 18.1	2.2	0.50	71.3 ± 4.8##	—	—
BLH-T03-20	20	14.4	10.8	42.1	47.7 ± 18.7	2.5	0.11	62.5 ± 3.3##	13.5 ± 1.3	101
MR20-2	20	28.6	11.0	81.3	90.2 ± 19.9	2.6	0.57	64.4 ± 3.5##	13.6 ± 0.6	5
SR-RM-01	20	16.1	11.4	20.8	22.3 ± 13.3	2.5	0.5	148.3 ± 11.3##	13.6 ± 0.6	50
OC-C2	20	0.7	11.8	2.7	2.7 ± 0.9	2.5	1.00	55.9 ± 8.4##	—	—
Western Wyoming										
WDA-GV-2	20	5.7	11.5	23.2	24.6 ± 37.0	—	0.73	46.9 ± 4.7***	—	—
GV18-1	22	2.9	10.5	9.7	11.3 ± 6.4	—	0.34	51.2 ± 5.1***	—	—
GV18-2	14	10.4	10.6	32.2	36.9 ± 19.2	—	0.98	56.0 ± 4.7***	—	—
GV18-3	22	4.1	10.8	14.7	16.7 ± 7.5	—	0.97	48.5 ± 3.8***	—	—
GV18-4	5	10.4	10.6	32.2	36.9 ± 16.6	—	0.98	63.2 ± 14.2***	—	—
GV18-5	20	10.9	11.1	35.0	38.4 ± 19.4	—	0.98	56.4 ± 4.3***	—	—
GV18-6	20	14.4	11.3	45.9	49.8 ± 19.9	—	0.36	57.5 ± 4.2***	—	—
GRL17-1	20	8.0	14.5	32.4	27.4 ± 16.7	—	0.95	58.3 ± 3.0***	—	—
WR18-1	20	6.7	11.6	24.2	25.4 ± 12.2	—	1.00	52.1 ± 4.3***	—	—
WR18-2	20	8.2	11.8	26.4	27.4 ± 14.5	—	0.47	59.1 ± 4.7***	—	—
SPASS1-2	12	8.2	14.1	33.0	28.5 ± 11.1	—	0.22	57.2 ± 5.3***	—	—
WR2	20	1.8	10.0	5.0	6.0 ± 2.3	—	0.58	59.5 ± 6.3***	—	—
WR1	20	2.0	10.1	8.4	10.1 ± 4.5	—	0.49	38.6 ± 3.7***	—	—

*Number of grains analyzed per sample.
†Density of spontaneous tracks counted.
§Density of dosimeter tracks counted.
#Density of induced tracks counted.
**Mean concentration of ^{238}U.
††Mean length of the etch pits in μm.
§§Probability that single grain ages belong to the same population.
##Samples counted by Gilby Jepson (GJ), ζ-value of 341.6 (8.5).
***Samples counted by Walter D. Afonso (WDA), ζ-value of 326.9 (8.9).
†††Mean track length.
§§§Number of confined fission tracks.

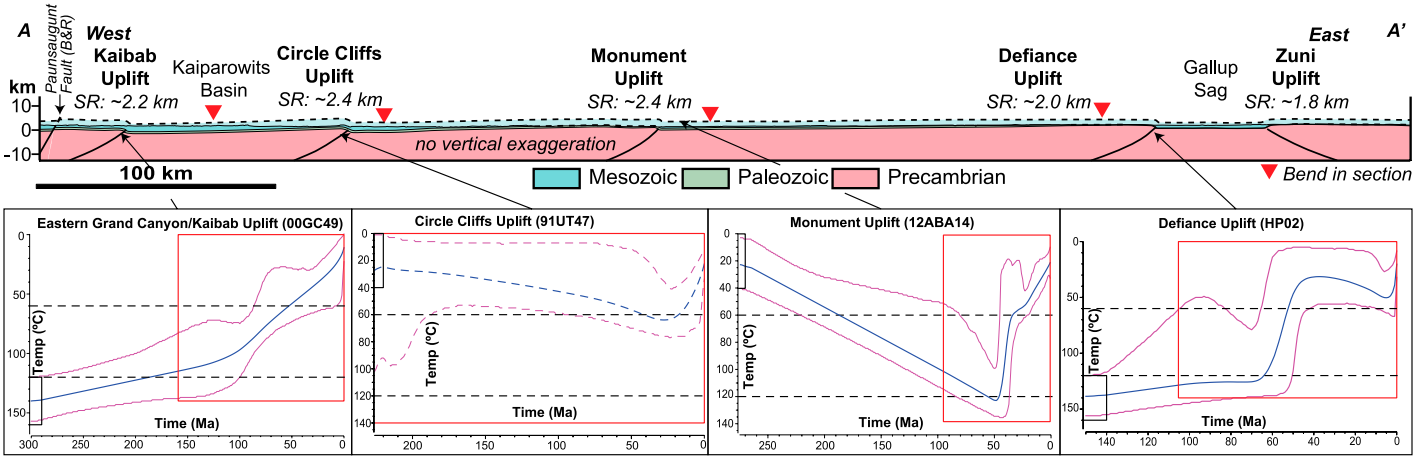

Figure 2. Thermal history models for Southern Transect, southwestern Colorado Plateau–southeastern Wyoming (Fig. 1, A–A′). Black squares indicate starting point of thermal history model; red box shows the extent of time-temperature sensitivity. B&R—Basin and Range; SR—structural relief.

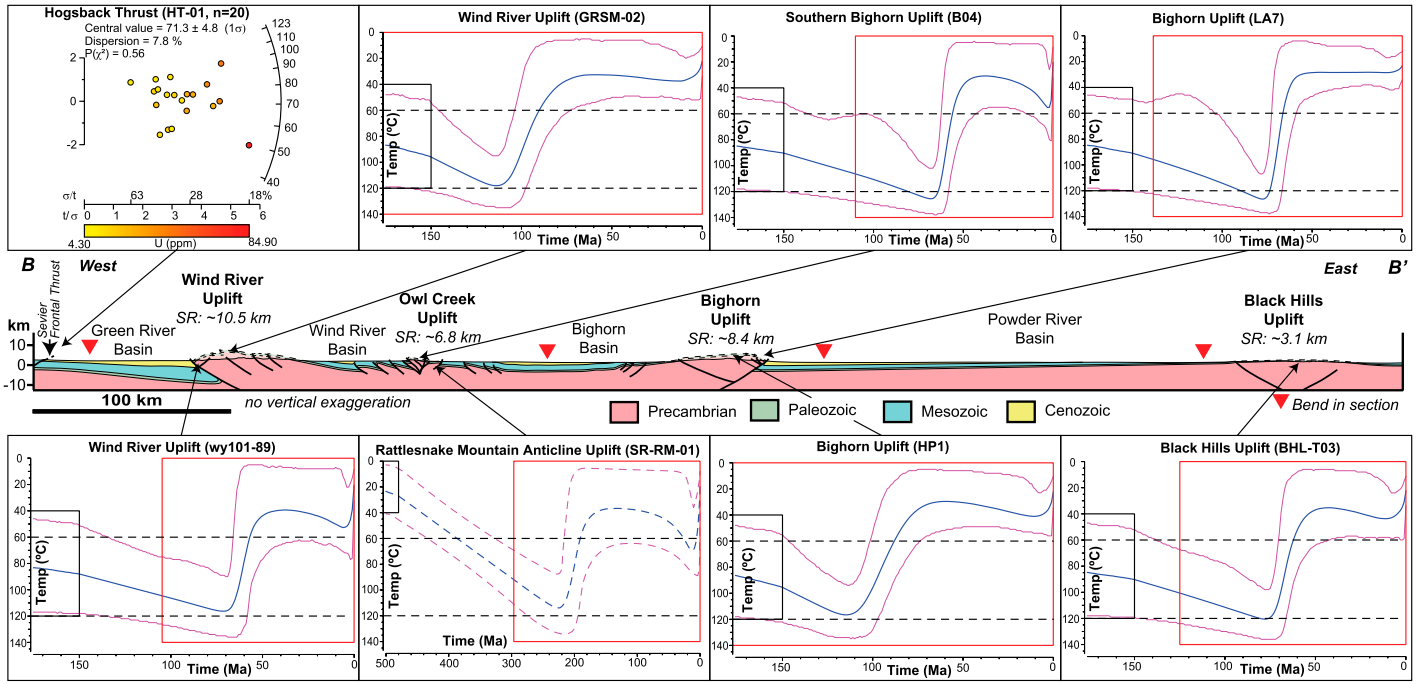

Figure 3. Thermal history models for Transect Two, northern Wyoming–South Dakota (B–B′). Black squares indicate starting point of thermal history model; red box shows the extent of time-temperature sensitivity. SR—structural relief.

and structural contacts, bedding attitudes, and stratigraphic thicknesses reported on published geologic maps (Doelling, 2008; Hackman and Olson, 1977; Hackman and Wyant, 1973; Haynes et al., 1972; Love and Christiansen, 1985; O'Sullivan and Beikman, 1963; Redden and DeWitt, 2008; Wyoming State Geological Survey, 2022), and publicly available well log data (Utah Division of Oil Gas and Mining, https://oilgas.ogm.utah.gov/oilgasweb/live-data-search/lds-main.xhtml [accessed March 2021]; Wyoming Oil and Gas Conservation Commission, https://dataexplorer.wogcc.wyo.gov/ [accessed February 2022]). The eastern portion of the Wyoming cross section was influenced by previous structural interpretations by Stone and Hollberg (1987). Geometries of nonemergent basement faults were determined with trishear fault-fold relationships with algorithms (e.g., Zehnder and Allmendinger, 2000) from Erslev (1991) built into Petex Move software exploiting geometric constraints of the deformed sedimentary cover.

RESULTS

Apatite Fission-Track Dating

Twenty-nine samples were collected from Laramide structures across Wyoming, Colorado, and South Dakota (Fig. 1). These samples are subdivided into northern Colorado–southern Wyoming, northern Wyoming–South Dakota, and western Wyoming (Table 2). Samples from the Gros Ventre uplift, western Wyoming (n = 13) yielded AFT central ages between 63 Ma and 49 Ma (Table 2). Samples from the Sweetwater uplift, central Wyoming (n = 6) yielded AFT central ages between 72 Ma and 59 Ma (Table 2). Samples from the Snowy–Sierra Madre uplift in northern Colorado–southern Wyoming (n = 4) yielded a range of AFT central ages between 89 Ma and 70 Ma (Table 2). Samples from northern Wyoming–South Dakota (n = 5) yielded AFT central ages between 71 Ma and 55 Ma, with an outlier age of ca. 148 Ma (SR-RM-01, Table 2). Finally, samples (n = 13) from western Wyoming yielded AFT central ages between 60 Ma and 38 Ma (Table 2). Confined track lengths were measured when available; samples yielded a range of relatively long MTLs between ~13.3 μm and ~14.4 μm (Table 2).

Apatite (U-Th-Sm)/He Dating

Seven samples from western Wyoming were selected for AHe dating. Five single-grain aliquots were measured for each sample and yielded mean squared weighted deviation (MSWD) ages between 80 Ma and 30 Ma (Table 3). Samples GV18-3 and GV18-4 yielded single-grain AHe ages that are significantly older than the remaining single-grain age distribution (Table 3). A number of factors are invoked to explain single-grain AHe age dispersion such as radiation damage, spherical equivalent grain radius, grain fragmentation, U-Th zonation, U- and Th-bearing inclusions, He implantation, chemical composition, and crystal imperfections (e.g., Shuster et al., 2006; Fitzgerald et al., 2006; Brown et al., 2013; Wildman et al., 2016; Gerin et al., 2017). Given that many, if not all, of these factors can contribute to increasing a single-grain AHe age (Guo et al., 2021; He et al., 2021), we exclude the significantly older and outlier AHe ages (n = 2) from further interpretation.

INTERPRETATION

Thermal history modeling was conducted using samples along two structural transects (Figs. 2 and 3). The Southern Transect (A–A′, Fig. 1) runs through the central Colorado Plateau, a physiographic region that covers Utah, Colorado, Arizona, and New Mexico (thick black outline in Fig. 1). The Northern Transect (B–B′, Fig. 1) runs from western Wyoming to western South Dakota across the northern Laramide province (Fig. 3). Thermal history models for the Southern and Northern Transects are presented in Figures 2 and 3; single-grain apatite data and thermal history model metadata are available in Tables S2 and S3 and Figure S2.

In order to achieve a suitable coverage of cooling histories, samples from this study were integrated with previously published AFT and

TABLE 3. APATITE (U-Th-Sm)/He DATA FROM LARAMIDE UPLIFTS IN WYOMING (USA)

Sample	*n**	U (ppm)	Th (ppm)	Sm (ppm)	eU†	FT§	^{4}He (nmol/g)	Mass (g)#	Raw age (Ma)	Corr. age ± 1σ (Ma)
GV18-1	1	34.2	32.1	524.4	41.7	0.754	12.8	4.74E-06	55.7	74.2 ± 1.2
	1	49.7	50.1	668.8	61.5	0.766	17.2	6.45E-06	50.9	66.9 ± 1.1
	1	28.8	19.1	351.2	33.3	0.763	9.1	4.66E-06	49.7	65.4 ± 1.1
	1	21.8	32.4	708.5	29.4	0.814	8.2	8.42E-06	50. 3	62.0 ± 1.0
	1	51.6	78.3	707.6	70.0	0.774	18.9	6.25E-06	49.2	64.1 ± 1.0
64.5 ± 2.0 Ma										
GV18-2	1	42.2	34.1	449.5	50.2	0.705	17.6	2.76E-06	59.1	91.4 ± 1.1
	1	54.6	43.1	504.5	64.7	0.696	18.0	3.13E-06	51.1	73.7 ± 0.9
	1	40.3	60.9	628.9	54.6	0.68	14.0	1.86E-06	177.2	69.3 ± 0.8
	1	65.7	57.3	592.7	79.1	0.654	26.3	1.75E-06	52.0	93.8 ± 1.2
	1	58.9	41.6	467.1	68.7	0.707	22.7	3.07E-06	45.6	85.9 ± 1.0
80.1 ± 1.8 Ma										
GV18-3	1	23.0	12.5	567.9	26.0	0.741	8.5	4.03E-06	21.5	79.6 ± 1.0
	1	19.4	9.3	353.9	21.6	0.782	6.1	7.58E-06	13.3	65.4 ± 0.8
	1	*20.2*	*12.5*	*559.8*	*23.1*	*0.676*	*23.1*	*1.76E-06*	*21.0*	*260.8 ± 3.2*
	1	33.2	18.7	738.5	37.6	0.648	10.8	1.56E-06	40.0	80.2 ± 1.0
	1	21.3	13.3	517.6	24.4	0.647	6.2	1.56E-06	23.1	70.5 ± 0.9
72.8 ± 1.8 Ma										
GV18-4	1	145.7	102.3	397.6	169.8	0.697	14.7	2.56E-06	16.0	23.2 ± 0.3
	1	*2.4*	*48*	*37.6*	*13.7*	*0.791*	*50.0*	*5.19E-06*	*653.5*	*844.6 ± 24.8*
	1	0.4	15.3	111.6	4.1	0.75	0.8	2.67E-06	33.5	46.1 ± 0.8
	1	1.0	4.3	106.0	2.0	0.572	0.2	7.97E-07	19.9	35.3 ± 4.1
	1	7.6	6.5	227.1	9.2	0.767	2.5	3.18E-06	49.8	64.9 ± 0.9
42.3 ± 1.5 Ma										
GV18-5	1	25.5	4.5	350.2	26.5	0.809	8.3	1.00E-05	57.1	70.5 ± 0.9
	1	31.5	4.8	317.3	32.6	0.718	9.3	2.76E-06	52.0	72.3 ± 1.0
	1	22.4	4	228.8	23.3	0.743	7.0	3.62E-06	55.1	74.1 ± 1.0
	1	16.1	0.7	264.0	16.3	0.733	4.3	2.74E-06	47.5	64.5 ± 0.9
	1	18.8	0.7	337.7	19.0	0.781	5.6	5.68E-06	52.8	67.4 ± 1.0
69.9 ± 1.6 Ma										
GV18-6	1	52.3	18.3	317.1	56.6	0.775	15.5	1.89E-07	50.2	64.9 ± 0.8
	1	57.0	33	587.2	64.8	0.737	16.4	4.65E-08	46.3	63.1 ± 0.8
	1	49.1	18.1	651.4	53.4	0.707	14.5	5.67E-08	49.5	70.1 ± 0.9
	1	59.0	22.7	678.7	64.3	0.761	17.7	4.28E-08	50.2	66.0 ± 0.9
	1	61.7	27.9	817.7	68.3	0.687	17.2	9.16E-08	45.9	66.9 ± 0.9
66.0 ± 1.6 Ma										
GV18-7	1	81.3	38.9	403.0	90.4	0.822	25.5	1.09E-05	51.9	63.2 ± 1.1
	1	76.4	62.1	344.0	91.0	0.805	24.5	1.02E-05	49.5	61.8 ± 1.0
	1	99.0	92.7	497.0	121.0	0.797	33.8	8.84E-06	51.5	64.9 ± 1.1
	1	59.8	40.9	365.4	69.4	0.806	19.5	1.07E-05	51.5	64.2 ± 1.1
	1	59.7	42.5	427.5	69.7	0.768	17.9	5.86E-06	47.0	61.5 ± 1.1
63.1 ± 1.8 Ma										
DUR	1	—	—	—	—	1	—	1.57E-06	—	28.6 ± 0.4
	1	—	—	—	—	1	—	1.25E-05	—	30.8 ± 0.4
	1	—	—	—	—	1	—	8.59E-06	—	29.6 ± 0.4
	1	—	—	—	—	1	—	2.47E-06	—	31.9 ± 0.5
30.1 ± 1.8 Ma										

Note: Samples in italics are excluded from further interpretation. Corr. age—corrected age.
*Number of grains per aliquot.
†Effective uranium scaled for relative alpha production rate (U [ppm] + 0.235 × Th [ppm]).
§Alpha-ejection correction after Farley, 2002.
#Mass weighted average radius of apatite crystals measured in the aliquot analyzed.

AHe ages described below. Samples for thermal history modeling were selected based on their location relative to major fault (i.e., structurally highest and lowest samples with closest proximity), prior interpretation from published literature, and availability of single-grain (U-Th-[Sm])/He and fission-track data. When single-grain fission-track data were not provided, we produced synthetic data that matched the central age and uncertainty, MTL, and reported distribution. Thermal history models are reported spatially from west to east along the two transects.

Southern Transect

Thermal history model 00GC49 from the eastern Grand Canyon (Fig. 2) uses AFT data from Kelley and Karlstrom (2012). This model indicates slow cooling from ca. 120 Ma until the present day. Thermal history model 91UT-147 from the Circle Cliffs includes AFT data from Dumitru et al. (1994) and independent geological constraints (depositional age) and shows heating from ca. 200 Ma to ca. 50 Ma and a prolonged period of minor cooling from the mid Miocene until present day. The thermal history models from the eastern Grand Canyon and Kaibab uplift (Fig. 2) indicate relatively, slow monotonic cooling from ca. 150 Ma to ca. 50 Ma. Although the western Colorado Plateau

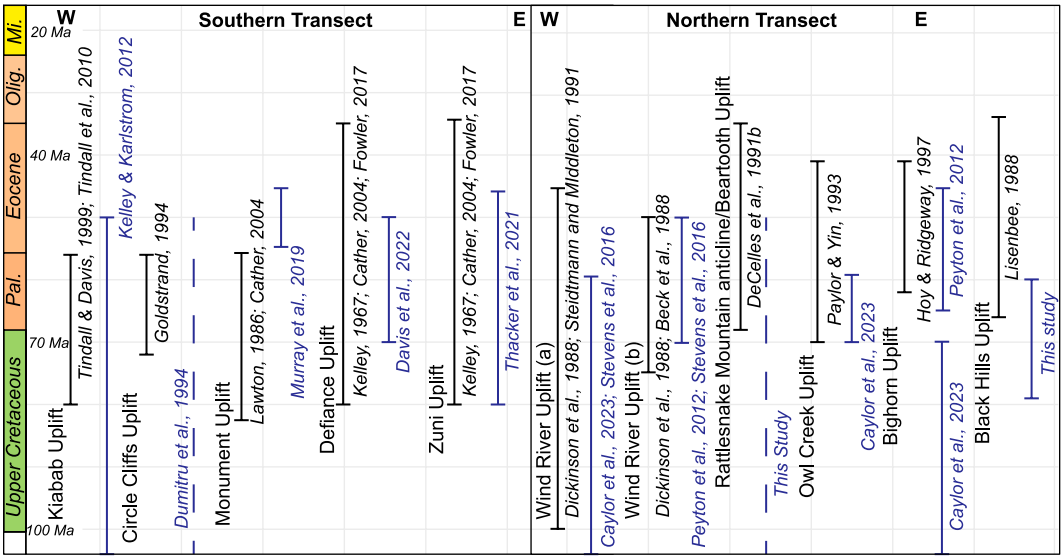

Figure 4. Temporal constraints and associated citations as defined by the stratigraphy and thermal history modeling from major Laramide uplifts along the Southern and Northern Transects. Black lines indicate timing constraints through sedimentological correlations. Uplift exhumation via thermal history constraints is in blue. Dashed lines indicate that no clear period of cooling was identified via thermal history modeling. Pal.—Paleocene; Olig.—Oligocene; Mi.—Miocene.

models suggest that exhumation may have initiated during the Early Cretaceous and continued steadily into Cenozoic time, the depositional record from the East Kaibab area indicates nonmarine conditions by ca. 80 Ma (Fig. 4; e.g., Leckie et al., 1991; Tindall et al., 2010). The burial record coupled with slow, monotonic thermal history models suggests that these ages are more likely a "mixed-age" as a result of incomplete thermal resetting during protracted burial (Gleadow et al., 1986). A mixed-age for the eastern Grand Canyon and Kaibab uplift is supported by thermal history modeling of sample 91UT-147 from the Circle Cliffs uplift showing only minor Cretaceous–Paleogene burial (Fig. 2; Dumitru et al., 1994). Much of the thermochronometric data from the western margin of the Colorado Plateau (Fig. 1) appear to be only partially reset through the apatite partial annealing zone and apatite partial retention zone, rendering interpretations of the Mesozoic–Cenozoic onset of Laramide exhumation based on thermal history models non-unique (Dumitru et al., 1994; Flowers et al., 2008; Karlstrom et al., 2017; Winn et al., 2017). Together, the thermal history models suggest that the western Colorado Plateau experienced a greater degree of reheating via burial compared to the Circle Cliffs region, but that the magnitude of burial was not enough to fully reset the AFT system.

Thermal history model 12ABA14 from Monument uplift (Fig. 2) includes geological constraints (depositional age), AFT, and AHe data from Murray et al. (2019) and shows reheating from ca. 250 Ma to 60 Ma, followed by enhanced cooling at ca. 60–35 Ma. The thermal history model for HP02 from the Defiance uplift (Fig. 2) includes AFT and AHe data from Davis et al. (2022) and shows a period of enhanced cooling at ca. 70–40 Ma (Figs. 2 and S2). The interior of the Colorado Plateau records a period of enhanced exhumation ca. 50 Ma (Fig. 2; Naeser et al., 2002; Murray et al., 2019). The thermal history model from sample 12ABA14 shows complete resetting prior to rapid cooling at ca. 50 Ma (Murray et al., 2019). The constraints on cooling provided by thermal history modeling are consistent with sedimentological evidence from the Mesaverde Group and the San Jose formation (Lawton, 1986; Cather, 2004; Fig. 4). However, they are significantly younger (ca. 50 Ma) than the proposed Campanian onset of Laramide-associated deposition in the San Juan basin (Lawton, 1986; Cather, 2004). Sample 12ABA14 is located to the east of the Monument uplift and is proximal to the La Sal laccolith, which yields zircon U-Pb ages of ca. 29 Ma (Rønnevik et al., 2017). Thus, cooling at ca. 50 Ma in the thermal history model could be partly the result of thermal disturbance of the AFT and AHe data by laccolith emplacement, a process that has been suggested to explain Oligocene–Miocene thermochronometric ages of samples from the Uncompahgre uplift (Fig. 2; Reiners, 2009; Rønnevik et al., 2017; Murray et al., 2019). However, an Eocene phase of exhumation in the Colorado Plateau interior is consistent with fault-gouge clays from the Uncompahgre uplift, which has been interpreted to represent fault displacement (Bailey et al., 2022). Eocene exhumation is also widely documented across the southern Colorado Plateau (Flowers et al., 2008; Karlstrom et al., 2022; Kapp et al., 2023). Finally, sedimentological and low-temperature thermochronometric datasets from the Defiance and Zuni uplifts in the southeastern Colorado Plateau also record Eocene exhumation (Fig. 2; Thacker et al., 2021; Davis et al., 2022). Thus, we suggest that the eastern half of the Colorado Plateau underwent a significant period of exhumation (up to ~3 km) at ca. 60–40 Ma.

Northern Transect

The Northern Transect runs from the western Wyoming to western South Dakota (B–B′, Fig. 1). The structural relief in the northern Laramide province is far greater than to the south. As a result, the thermochronometric data collected across Wyoming and Montana are more likely to record a broader range of Laramide cooling. Sample HT-01 (hanging wall of the Hogsback thrust) is from this study and yielded a cooling age of 71.3 ± 4.8 Ma, but insufficient confined-track lengths for thermal history modeling. The westernmost part of the cross section is through the Hogsback thrust, which marks the structural front of the Sevier fold-thrust belt. Shortening along the Hogsback thrust is well constrained by crosscutting and overlapping stratigraphic relationships to ca. 56–54 Ma. The AFT data from the Hogsback hanging wall, however, yield a cooling age of ca. 71 Ma (HT-01), which is too old to be explained by slip on the Hogsback thrust. However, the ca. 71 Ma age is broadly consistent with the age of uplift along the Laramide Moxa uplift, a subsurface west-vergent anticline that was erosionally beveled before the deposition of overlapping Campanian Ericson Formation (Devlin et al., 1993; Leary et al., 2015) and subsequently overlapped by the Hogsback thrust sheet (Lamerson, 1982; Coogan, 1992; DeCelles, 1994).

The thermal history model for wy101-89 for the Wind River uplift (Fig. 1) includes AFT data from Stevens et al. (2016) and shows enhanced cooling at ca. 70–50 Ma. The thermal history

model for GRSM-02 from the Wind River uplift includes AFT data from Caylor et al. (2023) and shows a period of enhanced cooling at ca. 110–80 Ma. The ca. 110–80 Ma onset of exhumation in the Wind River uplift is consistent with sedimentary evidence that places the onset of motion along the Wind River fault during the Late Cretaceous and deposition of the Frontier Formation in the western Bighorn Basin at ca. 99 Ma (Fig. 4; Steidtmann and Middleton, 1991; May et al., 2013). Sevier thrust belt flexural loading could have caused the observed subsidence. The Late Cretaceous onset of exhumation in western Wyoming is consistent with thermochronological data from western Montana, which have also documented 100–80 Ma exhumation (Omar et al., 1994; Carrapa et al., 2019; Ronemus et al., 2023). The Wind River uplift experienced a second period of exhumation at ca. 65–50 Ma (Fig. 3; Cerveny and Steidtmann, 1993; Stevens et al., 2016; Weil and Yonkee, 2023). Paleocene–Eocene cooling is consistent with rapid basin subsidence and extensive conglomerate deposition and is the dominant exhumation synorogenic signal preserved throughout the Wind River uplift (Steidtmann and Middleton, 1991; Cerveny and Steidtmann, 1993; Fan et al., 2011; Peyton et al., 2012; Stevens et al., 2016; Caylor et al., 2023).

The thermal history model for SR-RM-01 from the Rattlesnake Mountain anticline (Fig. 1; Bucher et al., 1933; Stearns, 1978; Erslev, 1993) uses AFT data from this study and yields a cooling history with an episode of slow, protracted heating from ca. 500 Ma to ca. 220 Ma, cooling from ca. 220 Ma to ca. 180 Ma, minor reheating (~20 °C) from ca. 100 Ma to ca. 15 Ma, and subsequent enhanced cooling from ca. 15 Ma to present day. The thermal history model from the Rattlesnake Mountain Anticline shows a tT path with cooling at ca. 250–200 Ma that is inconsistent with the Triassic strata preserved along the anticline margins (e.g., Neely and Erslev, 2009; Beaudoin et al., 2012). Thus, we interpret this AFT age as a mixed-age (a mixture of two cooling histories), reflecting incomplete resetting of the AFT system prior to Laramide-associated exhumation, similar to what is documented in samples from the western Colorado Plateau (sample 91UT147).

The thermal history model for sample B4 from the southwestern Bighorn uplift (Fig. 1) includes AFT data from Caylor et al. (2023) and shows a period of enhanced cooling from ca. 65 Ma to 45 Ma, minor reheating (~20 °C) at ca. 40–10 Ma, and Neogene cooling to surface temperatures. The thermal history model for sample HP1 (distal to the Clear Creek thrust system; Hoy and Ridgway, 1997) from the Bighorn uplift includes AFT data from Caylor et al. (2023) and shows a period of enhanced cooling from ca. 110 Ma to 65 Ma. Sample LA7 (proximal to the Clear Creek thrust system; Hoy and Ridgway, 1997) from the Bighorn uplift includes AFT data from Caylor et al. (2023) and shows a single period of enhanced cooling at ca. 80–60 Ma. The Late Cretaceous cooling signal is older than the timing of erosion recorded by Eocene conglomerate deposition in the western Powder River basin (Hoy and Ridgway, 1997). However, conglomerate deposition during the Eocene constrains the time at which the Archean granitic basement was exposed at the surface (Hoy and Ridgway, 1997) and may not capture the earlier erosional history. Peyton et al. (2012) noted that the conglomerate units were deposited upon angular basal unconformities, and thus, a considerable amount of exhumation may have occurred prior to conglomerate deposition (DeCelles et al., 1991b). Given that the isopach patterns of the Paleocene strata in the Powder River basin are indicative of initial uplift (Heller and Liu, 2016; Hoy and Ridgway, 1997) and sample HP1 is distal to the Clear Creak thrust system, our signal may represent the erosional product caused by Late Cretaceous exhumation preserved in the Powder River basin. In addition, some amount of cooling may occur during rock uplift and may pre-date erosion (ter Voorde et al., 2004). Here, we suggest that the Bighorn uplift underwent a period of initial exhumation or fault-induced cooling at ca. 100–90 Ma, consistent with previous thermochronometric investigations of the range (Crowley et al., 2002; Peyton et al., 2012; Caylor et al., 2023). The second phase of Paleocene–Eocene cooling at ca. 70–50 Ma in the Bighorn uplift is consistent with erosion recorded by conglomerate deposition (Dickinson et al., 1988; Hoy and Ridgway, 1997) and the bulk of the low-temperature thermochronometric data (Crowley et al., 2002; Peyton et al., 2012; Caylor et al., 2023).

The thermal history model for BHL-T03 from the Black Hills (Fig. 1) uses AFT data from this study and shows a period of enhanced cooling at ca. 75–50 Ma. A ca. 75–50 Ma period of exhumation is consistent with sedimentary constraints provided by the Fort Union and Wasatch Formations (Fig. 4; Lisenbee, 1988). Finally, five of the seven thermal history models from the Northern Transect show a period of minor reheating at ca. 40–10 Ma (Fig. 3). We suggest that this is due to a regional period of Cenozoic basin fill and subsequent evacuation consistent with Caylor et al. (2023).

Stratigraphic and Structural Constraints of Laramide Exhumation

Timing of exhumation of basement-cored uplifts throughout the Laramide province has long been constrained via sedimentological evidence prior to widespread application of low-temperature thermochronometric dating (e.g., Dorr et al., 1977; Nichols et al., 1985; Graham et al., 1986; DeCelles et al., 1987, 1991b; Dickinson et al., 1988; Crews and Etheridge, 1993; Hoy and Ridgway, 1997; Fan et al., 2011). To augment thermal history models of basement-involved uplifts, we compiled sedimentological and structural evidence from Laramide basins along our two transects.

The Southern Transect (A–A′ in Fig. 1; Fig. 2) starts with the eastern Grand Canyon (model 01GC87). Few sedimentary constraints are preserved near the Grand Canyon samples. However, the widespread occurrence of Cretaceous marine sedimentary rocks on the plateau is evidence that parts of the Colorado Plateau must have been below sea level until the Late Cretaceous (e.g., Leckie et al., 1991). The more proximal Kaiparowits Plateau preserves a combination of Santonian–Campanian shoreface, fluvial, and alluvial-fan deposits associated with active tectonics and source exhumation (Shanley and McCabe, 1991; Gooley et al., 2016). However, there are no clear sedimentological constraints on the Cretaceous–Paleogene exhumation of the western Colorado Plateau (Flowers et al., 2008; Winn et al., 2017). The Kaibab uplift preserves depositional and folding relationships that constrain initiation of surface uplift to the Campanian and cessation to the Paleocene (Tindall and Davis, 1999; Tindall et al., 2010). Dynamic topography models suggest that the Kaibab region was uplifted to low elevations (~500 m) by ca. 84 Ma (Heller and Liu, 2016). The Circle Cliffs uplift (model 91UT-147) preserves a depositional contact that constrains the initiation of exhumation to the Maastrichtian and cessation to the Paleocene (Goldstrand, 1994). The Uncompahgre uplift preserves depositional and folding relationships that broadly constrain the initiation of exhumation to the Late Cretaceous with cessation during the Eocene (Stone, 1977; Jamison and Stearns, 1982). Deposition of the Mesaverde Group suggests that exhumation of the Monument uplift initiated during the Campanian with cessation in the Paleocene (Lawton, 1986). The Defiance uplift preserves a broad record of exhumation with initiation at ca. 75 Ma and cessation as late as the late Eocene (Kelley, 1967; Fowler, 2017; Davis et al., 2022).

The Northern transect (western Wyoming to eastern South Dakota; B–B′ in Figs. 1 and 3) starts with the Hogsback thrust in the frontal part of the Sevier fold-thrust belt. Synorogenic sedimentation constrains latest fault slip on the Hogsback thrust to ca. 56–50 Ma (Royse et al., 1975; Coogan, 1992; DeCelles, 1994). Synorogenic deposits in the Green River Basin constrain

initial exhumation of the Wind River uplift to Maastrichtian and cessation to the mid-Eocene (Dickinson et al., 1988; Steidtmann and Middleton, 1991; Fan et al., 2011; Fan and Carrapa, 2014). In the western part of the Green River basin, the subsurface Moxa uplift, a basement-involved Laramide uplift, is erosionally truncated by Late Campanian (ca. 75–74 Ma) strata (Devlin et al., 1993; Leary et al., 2015). Stratigraphic relations in and around the Rock Springs uplift in the southern Green River basin demonstrate prolonged structural activity of the dome from Early Campanian through early Eocene time (Roehler, 1993; Mederos et al., 2005; Finn and Johnson, 2005; Leary et al., 2015). Initiation of uplift along the Rattlesnake Mountain anticline is documented to be Paleocene in age by the deposition of the synorogenic Beartooth conglomerate and Fort Union Formation, with cessation occurring variably during the Eocene (DeCelles et al., 1991a, 1991b). The southwestern Bighorn uplift preserves coarse-grained fluvial clastic rocks that constrain uplift initiation to the Maastrichtian and volcanic and volcaniclastic rocks bracket its cessation to the mid-Eocene (Dickinson et al., 1988; Paylor and Yin, 1993). The Bighorn uplift preserves depositional contacts that constrain initiation of exhumation to the middle Paleocene and cessation to the middle Eocene (Hoy and Ridgway, 1997; Caylor et al., 2023). The Black Hills uplift in eastern South Dakota preserves a depositional contact that constrains initiation of exhumation to the early Paleocene based on increased sand abundance, with cessation in the Oligocene due to the presence of flat-lying siltstones and tuffs (Lisenbee, 1988). Finally, in southwest Montana, a growth structure named the Maastrichtian Sphinx Conglomerate documents the timing of uplift of the Madison-Gravelly uplift (DeCelles et al., 1987) and the syntectonic Campanian Lima Conglomerate provides a constraint on the uplift and erosion of the Blacktail-Snowcrest uplift (Nichols et al., 1985; Haley, 1986).

DISCUSSION

Temporal and Spatial Patterns of Exhumation

The timing of Laramide deformation has traditionally been considered to be from the Maastrichtian to the middle Eocene (Dickinson et al., 1988). However, recent work suggests that exhumation of northern Laramide uplifts may have initiated as early as ca. 100–80 Ma (Carrapa et al., 2019). This is consistent with deposition of the ca. 86–78 Ma syntectonic Lima Conglomerate derived from Laramide uplifts in southwestern Montana (Nichols et al., 1985), a ca. 99–88 Ma maximum depositional age for the Ceno-Turonian Frontier Formation derived from detrital zircon samples from the eastern Beartooth uplift (May et al., 2013), and an 87–85 Ma age for unroofing of the Blacktail-Snowcrest uplift (Finzel et al., 2023). The ca. 100–80 Ma subsidence and concomitant exhumation cannot be explained by Sevier belt deformation propagating into the region because the ages reported by Carrapa et al. (2019) are exclusively from Laramide basement uplifts in southwest Montana and northwest Wyoming. A change from mostly flexural to flexural and dynamic subsidence at ca. 81 Ma suggests a switch to flat-slab subduction within the northern Laramide province at this time (e.g., Painter and Carrapa, 2013; May et al., 2013; Heller and Liu, 2016; Finzel et al., 2023). To explore the regional timing of exhumation across the Laramide province, we produced a kernel density estimate of all low-temperature thermochronometric ages between 150 Ma and 30 Ma (Fig. 5A). We observe that the Laramide province transitions from low frequency of cooling ages to a period of high frequency of cooling ages at ca. 100–80 Ma (Fig. 5A). The preservation of highly dispersed AFT cooling ages prior to 100 Ma matches age-elevation relationships from the Beartooth, Bighorn, Wind River, and Laramie uplifts. Omar et al. (1994) and Peyton et al. (2012) both identified that AHe and AFT data from the Bighorn and Beartooth uplifts show increased age dispersion and short confined-track lengths prior to 100 Ma, typically preserved at higher elevations and associated with slow, pre-Laramide cooling

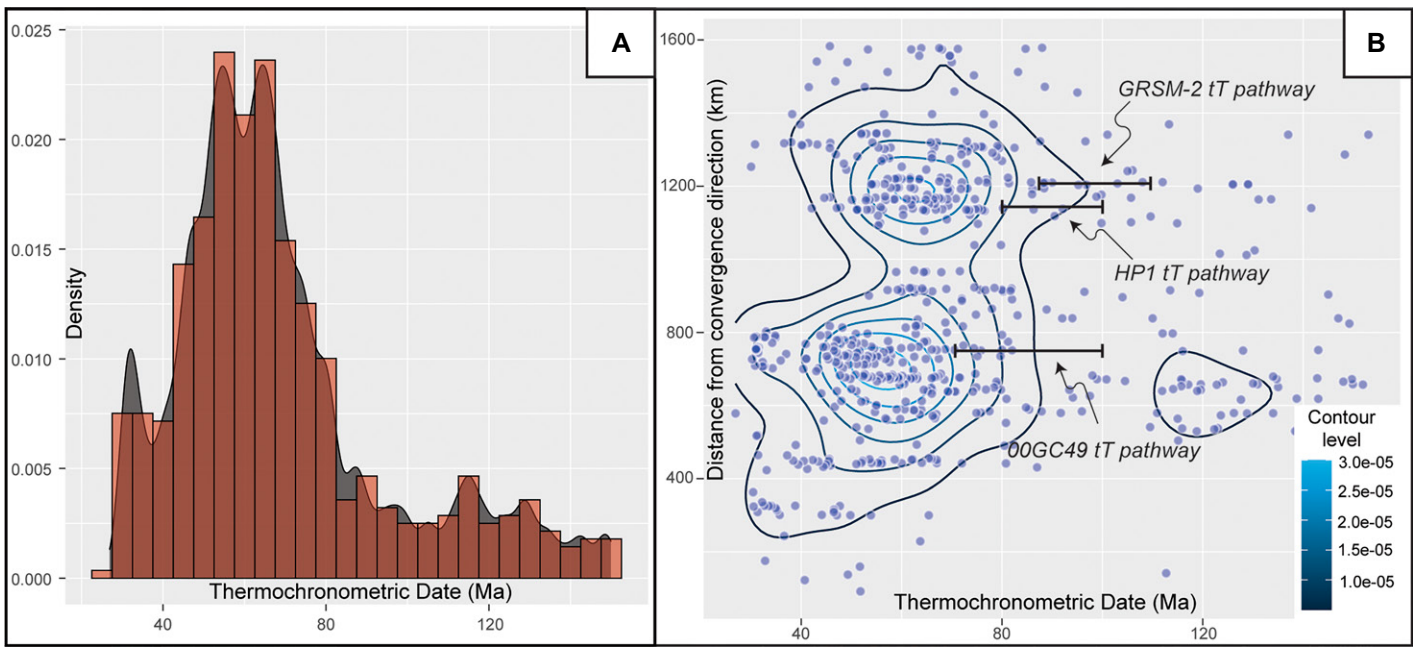

Figure 5. (A) Kernal density estimate of all thermochronometric ages for the Laramide province indicating an increase in density at ca. 90–80 Ma. (B) Contoured density plot of thermochronometric age by orthogonal distance relative to the Farallon–North America convergence direction (orange arrow, Fig. 1) after Copeland et al. (2017) and Torsvik et al. (2019). tT is time-temperature history as defined in Figure 3. A version of this figure that only uses apatite fission-track data with mean track lengths >13 µm is available as Figure S3 (see text footnote 1).

due to low-magnitude exhumation or prolonged residence in the apatite partial annealing zone and apatite partial retention zone. Furthermore, several studies have documented a distinct change from relatively slow to fast cooling, longer track lengths, and low age-elevation variation from ca. 100 Ma to 80 Ma associated with the initiation of deformation and exhumation in the northern Laramide uplifts (Peyton et al., 2012; Ronemus et al., 2023). The occurrence of ca. 100–80 Ma exhumation ~300–500 km to the east of the Sevier thrust front (Fig. 3) supports a change in the style of deformation and initiation of Laramide tectonics at this time. The dominant timing of cooling preserved across the Laramide province is ca. 70–50 Ma, yielding ~43% of the low-temperature thermochronometric ages (Fig. 5). The Late Cretaceous–Eocene peak is consistent with the majority of sedimentological and structural constraints from uplifts throughout the Laramide province (Fig. 4; Dickinson et al., 1988; DeCelles, 2004; Saylor et al., 2020; Weil and Yonkee, 2023). This signature is consistent with relatively rapid cooling across a broad area from New Mexico and Arizona (Kelley and Chapin, 1997; Caylor et al., 2021) to north-central Montana (Figs. 2 and 3; Bryant and Naeser, 1980; Cerveny and Steidtmann, 1993; Kelley and Chapin, 2004; Stevens et al., 2016; Howlett et al., 2024). Thus, the 70–50 Ma period of cooling is interpreted to represent the main phase of exhumation associated with Laramide-related deformation (e.g., Crowley et al., 2002; Kelley and Chapin, 2004; Weil and Yonkee, 2023).

The two principal models for the migration of the Farallon slab suggest either a SSW to NNE (~015°) path with earlier exhumation in the south (Saleeby, 2003), or a WSW to ENE (~065°) path with an irregular plate geometry allowing for earlier exhumation to the north (Fig. 1; Cross, 1986; Bird, 1998). A variety of plate convergence velocities are permissible in the Late Cretaceous–Paleocene, with those based on Kula-Pacific rotations following a SSW-NNE trajectory, and those based on Farallon plate rotations favoring a more WSW-ENE trajectory (e.g., Doubrovine and Tarduno, 2008; Torsvik et al., 2019). Assuming that contractional deformation associated with the flat slab is the major driver behind exhumation (e.g., Schildgen et al., 2018), each of these pathways makes specific predictions for the temporal distribution of low-temperature thermochronology. The SSW-NNE model (Saleeby, 2003; Liu et al., 2010) would predict low-temperature thermochronology to be older in northern Arizona and younger toward the NNE (Wyoming–South Dakota) along a narrow corridor (Axen et al., 2018). The WSW to ENE model combined with a variable Farallon plate geometry (Fig. 1; Cross, 1986; Bird, 1998) allows for a more variable pattern of low-temperature thermochronometric ages and regional exhumation to extend across a broader area.

To test between these models, we compared low-temperature thermochronometric age against distance from the Farallon–North America convergence direction (Figs. 1, 5B, and S3; Copeland et al., 2017; Torsvik et al., 2019) with greater distances being in the northwest and shorter in the southeast at present day. Based on the earliest appearance of a 0.001% 2-D density contour, the increased thermochronometric age density initiates earliest in samples with greatest distance from the convergence (1200 km) vector at ca. 100 Ma, and youngs to the southeast with increased thermochronometric age density of ca. 80 Ma and ca. 70 Ma at distances of 800 km and 400 km, respectively (Fig. 5B). These first-order age-distance trends are inconsistent with the SSW-NNE model of a migrating flat-slab along a narrow corridor (Saleeby, 2003). The pattern of older thermochronometric ages in the north compared to the south, and the broad distribution of 70–50 Ma ages, is more congruent with the original flat-slab trajectory models and plate geometries proposed by Cross (1986) and Bird (1998). However, major caveats need to be considered with regard to these data. Considerable spread exists in thermochronometric ages, with a cluster of ages at ca. 120 Ma at 600–500 km distance from the plate convergence vector (Fig. 5). We suggest that the ca. 120 Ma cluster represents mixed-ages as recorded by shorter MTLs and broad track length distributions, indicative of prolonged residence in the partial annealing zone (e.g., Omar et al., 1994; Reiners and Farley, 2001; Kelley and Chapin, 2004; Peyton et al., 2012). The interpretation of ca. 120 Ma AFT ages as mixed ages is consistent with sedimentary data, which document that a large portion of the Laramide province was covered by the Western Interior Seaway until the end of the Cretaceous (e.g., Kauffman, 1985). The ca. 120 Ma cooling signal may also be partly the result of erosion from the eastward migration of the forebulge through the regional foreland basin prior to actual Laramide basement uplifts (DeCelles, 2004).

A longer duration of movement along Laramide faults, assuming continuous shortening, would promote greater denudation and remove the older mixed-age signal. Estimates of structural relief across the Laramide province suggest that there has been significantly less exhumation south of the Uinta uplift (1–3 km) compared to the north (3–10 km; Figs. 2 and 3). Marshak et al. (2017) showed similar north-south trends based on calculated basement structural relief estimates across Laramide faults. It should be noted that many of the Laramide uplifts are reactivated structures in which total structural relief is the sum of pre-Laramide and Laramide relief (e.g., Hoppin, 1961; Paylor and Yin, 1993; Bader, 2019). Structural relief estimates are consistent with detailed thermal history models that show that samples in the southern Colorado Plateau (e.g., Circle Cliffs and Eastern Grand Canyon) have not experienced sufficient exhumation to remove the record of older (older than 100 Ma) cooling (Fig. 2; Dumitru et al., 1994; Kelley and Karlstrom, 2012). An alternative mechanism for preservation of a mixed-age signal could be a stronger lower crust rheology beneath the Colorado Plateau (e.g., Rautela et al., 2020). Flexural rigidity and seismic velocity models, however, show a similar rheology between the Wyoming Craton and the Colorado Plateau at present (e.g., Lowry and Smith, 1995; Levander et al., 2011). Regardless of these local details, the regional structural relief estimates illustrate the relatively shallower exhumation in the southern Laramide province compared to the north, which we interpret as at least partially contributed to by an earlier onset of flat-slab associated deformation in the north.

In a regional synthesis of available structural, sedimentological, and low-temperature thermochronological data, Weil and Yonkee (2023) emphasize the ca. 75–50 Ma AFT ages in many of the northern Laramide uplifts as a record of Laramide-related cooling. The low-temperature thermochronometric data, which yield ages older than 75 Ma, are interpreted by these authors to reflect mixed-ages as a result of residence in the apatite partial annealing zone due to shallow burial. Following this approach, Weil and Yonkee (2023) suggest that exhumation initiated ca. 80 Ma in southwestern Utah and youngs to the northeast into Wyoming. Other low-temperature thermochronometric studies (Omar et al., 1994; Crowley et al., 2002; Peyton et al., 2012; Ronemus et al., 2023) have interpreted cooling ages older than 100 Ma to represent prolonged burial, slow cooling or mixed-ages. Our thermal history modeling shows that at least some samples are sufficiently annealed to record cooling at ca. 100–80 Ma. Coupled with sedimentary constraints, we suggest that the northern Laramide province underwent a two-stage exhumation history: an initial and more limited phase of exhumation at ca. 100–80 Ma, followed by a major and regionally widespread period of exhumation at ca. 70–50 Ma (Fig. 6). The Late Cretaceous and Paleocene–Eocene periods of exhumation observed in the Wind River, Bighorn, and Black Hills uplifts are consistent with what is observed in the Beartooth uplift (Omar et al., 1994; Peyton et al., 2012; Peyton and Carrapa, 2013; Carrapa et al., 2019; Ronemus

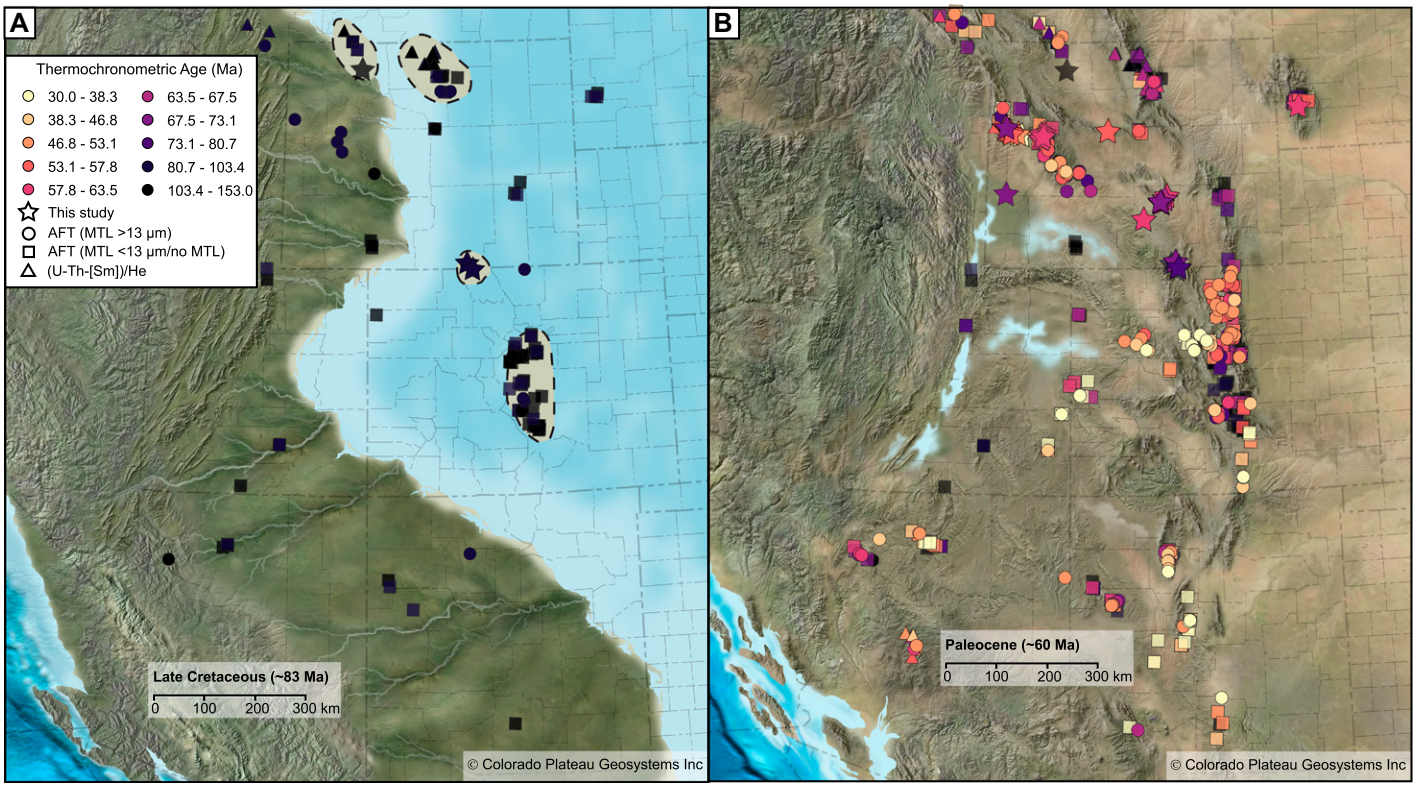

Figure 6. Paleogeographic maps during (A) Late Cretaceous and (B) Paleocene time after Blakey and Ranney (2017), modified to include thermochronological data and to show earlier onset of exhumation of the northern Laramide province. Circles are published apatite fission-track (AFT) samples with a mean track length (MTL) >13 µm, indicative of relatively rapid cooling. Squares are samples that have either MTLs <13 µm or no MTLs reported, indicative of relatively slow cooling or more complex cooling histories. Triangles are apatite and zircon (U-Th-[Sm])/He ages, and stars are samples from this study.

et al., 2023). The exhumation pattern is consistent with the regional Laramide basin subsidence record, which shows initial tectonic subsidence developing at ca. 100–80 Ma, followed by a more prominent period at ca. 75–60 Ma due to dynamic subsidence associated with shallowing of the Farallon slab (Heller and Liu, 2016). This two-stage thermal and exhumation history is inconsistent with models that seek to propagate deformation and exhumation along a narrow SSW-NNE corridor (e.g., Saleeby, 2003; Axen et al., 2018). Instead, we find the timing of northern Laramide exhumation is more consistent with a WSW to ENE trajectory and irregular plate boundary geometries, proposed by Cross (1986) and Bird (1998); however, this phase of deformation and exhumation initiated earlier and propagated in an episodic and spatially heterogeneous manner across a broader region than previously proposed.

Tectonic Mechanisms for Laramide Exhumation

Based on regional low-temperature thermochronology (Fig. 5) and thermal history models in the context of our regional cross sections (Figs. 2 and 3) we suggest that (1) the magnitude of exhumation in the northern Laramide province is greater than what is observed in the southern Laramide province, consistent with an earlier inception of Laramide deformation to the north, and (2) exhumation in the Laramide province occurred in two pulses, first during the Late Cretaceous and second during the Paleocene–Eocene. Based on the shut-off of the magmatic arc, inboard sweep of magmatism, and transition from thin-skinned to thick-skinned faulting and mostly flexural to flexural and dynamic subsidence, Laramide deformation has been interpreted as the result of flattening of the subducting Farallon slab and increased coupling between the down-going and overriding plates (e.g., Coney and Reynolds, 1977; Dickinson and Snyder, 1978; Weil and Yonkee, 2023). However, outstanding questions remain regarding how the Farallon slab coupled with the overriding North American plate as outlined in the introduction (Fig. 1). Here, we seek to assess various models of Laramide flat-slab subduction through an analysis of the distribution of regional exhumation within the Laramide province.

Flattening of the Farallon Plate

Livaccari et al. (1981) suggested that slab flattening could be facilitated by subduction of a buoyant oceanic plateau. Based on the present-day locations of the Shatsky and Hess rises (Henderson et al., 1984), the paleo-conjugates were suggested to have subducted beneath the North American plate at ca. 90–70 Ma (Shatsky) and at ca. 65–50 Ma (Hess), which is thought to have produced a general SW to NE younging pattern in the ages of individual Laramide uplifts (e.g., Liu et al., 2010). Our regional analysis of low-temperature thermochronological data from the Laramide province shows that there is both a timing and spatial inconsistency with the proposed trajectory for the Shatsky conjugate model. The timing of the putative Shatsky conjugate subduction agrees with the onset of uplift in the Colorado Plateau (ca. 80 Ma; Tindall et al., 2010; Thacker et al., 2023) but postdates the initiation of exhumation recorded in the northern Laramide province (ca. 100–80 Ma; Figs. 2, 3, and 5). Continued magmatism in the Southern California Batholith at ca. 90–70 Ma suggests a more limited footprint of the proposed Shatsky conjugate (Schwartz et al., 2023). Thus,

if the hypothesized plateau subduction model holds true, its timing requires an ~10 m.y. earlier initiation to satisfy the regional exhumation history resolved by low-temperature thermochronology and an almost synchronous propagation of exhumation to satisfy older ages (ca. 100–80 Ma) in Wyoming and Montana. The temporal inconsistency is compounded when we consider the spatial distribution of initial exhumation in the Laramide province. Several major Laramide uplifts (Wind River, Beartooth, and Bighorn) record initial exhumation at ca. 100–80 Ma, which is when the Shatsky conjugate plateau is proposed to have subducted far to the south beneath the southwestern Cordilleran margin (Saleeby, 2003). This pattern would have been difficult to achieve without invoking an independent geodynamic process. Further, low-temperature thermochronology from Kapp et al. (2023) suggests that the southern margin of the Colorado Plateau underwent significant exhumation at ca. 60–40 Ma. Neither of these time frames of exhumation is consistent with the Saleeby (2003) model.

Recent plate kinematic models for the Cretaceous to early Cenozoic evolution of large igneous provinces (LIPs) in the northwest Pacific basin provide updated possibilities for which, if any, conjugate plateaus could have collided with North America during the mid- to Late Cretaceous. Torsvik et al. (2019) provided adjustments to the Müller et al. (2016) plate kinematic model, and interpreted that all or most of the Shatsky Plateau was transferred by ridge jump onto the Pacific plate no later than 134 Ma. This implies that no significant conjugate to the Shatsky Plateau existed on the Farallon plate. Fletcher et al. (2020) reconsidered conventional mantle plume models and presented a reconstruction in which at least five LIP-related conjugate features on the Farallon plate collided with the western coast of California in two successive events from 85 Ma to 64 Ma and 67 Ma to 65 Ma. The earlier event occurred mainly at northern California latitudes, whereas the younger event occurred at more southerly latitudes; both sets of collisions had ENE trajectories. All of the conjugates in the Fletcher et al. (2020) model are thought to have been much smaller than previously assumed, consistent with Torsvik et al. (2019). Results of these studies are more consistent with our regional Laramide thermochronology signature than previous models invoking a Shatsky conjugate, with dimensions comparable to the Shatsky Plateau colliding at southern California latitudes with a NNE trajectory. This would largely remove the need for a single, large oceanic plateau to explain flat-slab subduction and would suggest that an increase in plate convergence velocity facilitated flattening of the Farallon slab and associated deformation (e.g., Bird, 1984). Although uncertainty persists, the velocity of the Farallon plate relative to North America as reconstructed from seafloor magnetic anomalies increased abruptly at ca. 100 Ma and ca. 75 Ma (e.g., Engebretson et al., 1984; Matthews et al., 2012; Liu and Currie, 2016). We suggest that a combination of increased convergence rates and the subduction of moderate to small oceanic edifices at northern and southern California latitudes can explain the spatial and temporal distributions of Laramide low-temperature cooling ages.

Basal-Shear versus End-Loading

Regardless of the precise mechanism for flattening of the Farallon slab, deformation was transmitted from the subducting slab to the upper-plate via increased coupling (e.g., Coney and Reynolds, 1977; Dickinson and Snyder, 1978). It has long been hypothesized that migration of the flattened Farallon slab would result in temporally coincident deformation (Henderson et al., 1984; Saleeby, 2003). Geodynamic models of the Farallon flat-slab suggest that deformation is progressively transferred to the upper-plate along its leading hinge via basal traction (Bird, 1998). The model of progressive deformation is supported by stratigraphic and limited low-temperature thermochronological evidence in the southern Laramide province (Thacker et al., 2023). However, when considering the entire Laramide province, we suggest that exhumation does not follow a coherent, spatial migration as posited by Bird (1998; Fig. 1). Rather, based on thermal history models along the two transects through the Colorado Plateau and Wyoming–South Dakota, we show that exhumation initiated in the region closest to the Sevier thrust front but then propagated rapidly into the interior of the Laramide province (Figs. 2 and 3). A mixture of both older (ca. 100–80 Ma) and younger (ca. 70–50 Ma) cooling ages consistent with rapid cooling is found in both the Laramie and Colorado Front uplifts and in the Beartooth and Wind River uplifts (e.g., Omar et al., 1994; Kelley and Chapin, 2004; Stevens et al., 2016; Caylor et al., 2023). This distribution of exhumation supports the end-loading model as defined by Erslev et al. (2022), in which deformation and exhumation propagate synchronously from the margin, far into the interior, perhaps facilitated by inherited structures (Schmidt et al., 1988; Schmidt and Garihan, 1983) and pre-shortening stratigraphic architecture (Bader, 2019; Parker and Pearson, 2021; Howlett et al., 2024).

CONCLUSIONS

Our compilation of published and new thermochronometric ages documents the spatial and temporal trends of regional exhumation across the Laramide province. We identify distinct periods of exhumation within the Laramide province. The first, initial exhumation at ca. 100–80 Ma, is mostly concentrated in the northern Laramide, temporally consistent with an increase in relative Farallon–North America plate velocity. The second, widespread and more rapid exhumation event at ca. 70–50 Ma, is temporally consistent with a second increase in relative Farallon–North America plate velocity. Both events may be correlated with subduction of two sets of oceanic edifies, rather than a single very large Shatsky Plateau conjugate. We find that the northern Laramide province (Montana-Wyoming) underwent higher magnitude and earlier (ca. 100 Ma) exhumation compared to the southern Laramide province (Utah-Arizona, ca. 75 Ma). The earlier initiation of deformation in the northern Laramide is consistent with the Bird (1998) trajectory and paleogeographic model for the flattened Farallon plate but broader in spatial extent. Finally, our thermal history models coupled with regional cross sections through the southern and the northern Laramide province show that exhumation occurred relatively synchronously across a broad region with no clear W-to-E trends. Thus, we suggest that deformation and exhumation occurred in response to end-loading rather than increased coupling during basal-shear.

ACKNOWLEDGMENTS

G. Jepson acknowledges support from National Science Foundation (NSF) grant EAR2419296. B. Carrapa and P.G. DeCelles acknowledge support from NSF grant EAR1919179. Reviewers Andrew Zuza and Adolph Yonkee, associate editor Tim Kusky, and science editor Wenjiao Xiao are thanked for their insightful comments, which helped us improve this work.

REFERENCES CITED

Allmendinger, R.W., 1992, Fold and thrust tectonics of the western United States exclusive of the accreted terranes, *in* Burchfield, B.C., Lipman, P.W., and Zoback, M.L., eds., The Cordilleran Orogen: Conterminous U.S.: Geological Society of America, Decade of North American Geology, Geology of North America, v. G-3, p. 583–608, https://doi.org/10.1130/DNAG-GNA-G3.583.

Armstrong, R.L., 1968, Sevier orogenic belt in Nevada and Utah: Geological Society of America Bulletin, v. 79, p. 429–458, https://doi.org/10.1130/0016-7606(1968)79[429:SOBINA]2.0.CO;2.

Axen, G.J., van Wijk, J.W., and Currie, C.A., 2018, Basal continental mantle lithosphere displaced by flat-slab subduction: Nature Geoscience, v. 11, p. 961–964, https://doi.org/10.1038/s41561-018-0263-9.

Bader, J.W., 2019, Structural inheritance and the role of basement anisotropies in the Laramide structural and tectonic evolution of the North American Cordilleran foreland, Wyoming: Lithosphere, v. 11, p. 129–148, https://doi.org/10.1130/L1022.1.

Bahadori, A., Holt, W.E., Feng, R., Austermann, J., Loughney, K.M., Salles, T., Moresi, L., Beucher, R., Lu, N., Flesch, L.M., and Calvelage, C.M., 2022, Coupled in-

fluence of tectonics, climate, and surface processes on landscape evolution in southwestern North America: Nature Communications, v. 13, https://doi.org/10.1038/s41467-022-31903-2.

Bailey, L.R., Kirk, J., Hemming, S.R., Krantz, R.W., and Reiners, P.W., 2022, Eocene fault-controlled fluid flow and mineralization in the Paradox Basin, United States: Geology, v. 50, p. 326–330, https://doi.org/10.1130/G49466.1.

Beaudoin, N., Leprêtre, R., Bellahsen, N., Lacombe, O., Amrouch, K., Callot, J.P., Emmanuel, L., and Daniel, J.M., 2012, Structural and microstructural evolution of the Rattlesnake Mountain Anticline (Wyoming, USA): New insights into the Sevier and Laramide orogenic stress build-up in the Bighorn Basin: Tectonophysics, v. 576–577, p. 20–45, https://doi.org/10.1016/j.tecto.2012.03.036.

Beck, R.A., Vondra, C.F., Filkins, J.E., and Olander, J.D., 1988, Syntectonic sedimentation and Laramide basement thrusting, Cordilleran foreland; timing of deformation, *in* Schmidt, C.J., and Perry, W.J., Jr., eds., Interaction of the Rocky Mountain Foreland and the Cordilleran Thrust Belt: Geological Society of America Memoir 171, p. 465-488, https://doi.org/10.1130/MEM171-p465.

Bellemans, F., De Corte, F., and Van Den Haute, P., 1995, Composition of SRM and CN U-doped glasses: Significance for their use as thermal neutron fluence monitors in fission track dating: Radiation Measurements, v. 24, p. 153–160, https://doi.org/10.1016/1350-4487(94)00100-F.

Best, M.G., Christiansen, E.H., de Silva, S., and Lipman, P.W., 2016, Slab-rollback ignimbrite flareups in the southern Great Basin and other Cenozoic American arcs: A distinct style of arc volcanism: Geosphere, v. 12, p. 1097–1135, https://doi.org/10.1130/GES01285.1.

Bird, P., 1984, Laramide crustal thickening event in the Rocky Mountain Foreland and Great Plains: Tectonics, v. 3, p. 741–758, https://doi.org/10.1029/TC003i007p00741.

Bird, P., 1998, Kinematic history of the Laramide orogeny in latitudes 35°–49°N, western United States: Tectonics, v. 17, p. 780–801, https://doi.org/10.1029/98TC02698.

Blackwelder, E., 1914, A summary of the orogenic epochs in the geologic history of North America: The Journal of Geology, v. 22, p. 633–654, https://doi.org/10.1086/622180.

Blakey, R.C., and Ranney, W.D., 2017, Ancient Landscapes of Western North America: A Geologic History with Paleogeographic Maps: Springer, 228 p., https://doi.org/10.1007/978-3-319-59636-5.

Braun, J., van der Beek, P., and Batt, G., 2006, Quantitative Thermochronology: Numerical Methods for the Interpretation of Thermochronological Data: Cambridge University Press, 258 p., https://doi.org/10.1017/CBO9780511616433.

Brown, R.W., Beucher, R., Roper, S., Persano, C., Stuart, F., and Fitzgerald, P., 2013, Natural age dispersion arising from the analysis of broken crystals. Part I: Theoretical basis and implications for the apatite (U-Th)/He thermochronometer: Geochimica et Cosmochimica Acta, v. 122, p. 478–497, https://doi.org/10.1016/j.gca.2013.05.041.

Brown, S.J., Thigpen, J.R., Spotila, J.A., Krugh, W.C., Tranel, L.M., and Orme, D.A., 2017, Onset timing and slip history of the Teton fault, Wyoming: A multidisciplinary reevaluation: Tectonics, v. 36, p. 2669–2692, https://doi.org/10.1002/2016TC004462.

Brown, W.G., 1988, Deformational style of Laramide uplifts in the Wyoming foreland, *in* Schmidt, C.J., and Perry, W.J., eds., Interaction of the Rocky Mountain Foreland and the Cordilleran Thrust Belt: Geological Society of America Memoir 171, p. 1–26, https://doi.org/10.1130/MEM171-p1.

Bucher, W.H., Chamberlin, R.T., and Thom, W.T., Jr., 1933, Results of structural research work in Beartooth-Bighorn Region, Montana and Wyoming: AAPG Bulletin, v. 17, p. 680–693, https://doi.org/10.1306/3D932B66-16B1-11D7-8645000102C1865D.

Burchfiel, B.C., and Davis, G.A., 1972, Structural framework and evolution of the southern part of the Cordilleran orogen, western United States: American Journal of Science, v. 272, p. 97–118, https://doi.org/10.2475/ajs.272.2.97.

Burchfiel, B.C., Cowan, D.S., and Davis, G.A., 1992, Tectonic overview of the Cordilleran orogen in the western United States, *in* Burchfiel, B.C., Lipman, P.W., and Zoback, M.L., eds., The Cordilleran Orogen: Conterminous U.S.: Geological Society of America, Decade of North American Geology, Geology of North America, v. G3, p. 407–414, https://doi.org/10.1130/DNAG-GNA-G3.407.

Bryant, B., and Naeser, C.W., 1980, The significance of fission-track ages of apatite in relation to the tectonic history of the Front and Sawatch Ranges, Colorado: Geological Society of America Bulletin, v. 91, p. 156–164, https://doi.org/10.1130/0016-7606(1980)91<156:TSOFAO>2.0.CO;2.

Camilleri, P.A., and Chamberlain, K.R., 1997, Mesozoic tectonics and metamorphism in the Pequop Mountains and Wood Hills region, northeast Nevada: Implications for the architecture and evolution of the Sevier orogen: Geological Society of America Bulletin, v. 109, p. 74–94, https://doi.org/10.1130/0016-7606(1997)109<0074:MTAMIT>2.3.CO;2.

Carlson, W.D., Donelick, R.A., and Ketcham, R.A., 1999, Variability of apatite fission-track annealing kinetics: I. Experimental results: American Mineralogist, v. 84, p. 1213–1223, https://doi.org/10.2138/am-1999-0901.

Carpenter, D.G., Carpenter, J.A., Dobbs, S.W., and Stuart, C.K., 1993, Regional structural synthesis of Eureka fold-and-thrust belt, east-central Nevada, *in* Gillespie, C.W., ed., Structural and Stratigraphic Relationships of Devonian Reservoir Rocks, East-Central Nevada: Nevada Petroleum Society, 1993 Field Conference Guidebook, p. 59–72.

Carrapa, B., DeCelles, P.G., and Romero, M., 2019, Early inception of the Laramide Orogeny in southwestern Montana and northern Wyoming: Implications for models of flat-slab subduction: Journal of Geophysical Research: Solid Earth, v. 124, p. 2102–2123, https://doi.org/10.1029/2018JB016888.

Cassel, E.J., Smith, M.E., and Jicha, B.R., 2018, The impact of slab rollback on Earth's surface: Uplift and extension in the hinterland of the North American Cordillera: Geophysical Research Letters, v. 45, https://doi.org/10.1029/2018GL079887.

Cather, S.M., 2004, Laramide orogeny in central and northern New Mexico and southern Colorado, *in* Mack, G.H., and Giles, K.A., eds., The Geology of New Mexico, A Geologic History: New Mexico Geological Society Special Publication 11, p. 203–248, https://doi.org/10.56577/SP-11.

Caylor, E., Carrapa, B., Jepson, G., Sherpa, T.Z., and DeCelles, P.G., 2023, The rise and fall of Laramide topography and the sediment evacuation from Wyoming: Geophysical Research Letters, v. 50, https://doi.org/10.1029/2023GL103218.

Caylor, E.A., Carrapa, B., Sundell, K., DeCelles, P.G., and Smith, J.M., 2021, Age and deposition of the Fort Crittenden Formation: A window into Late Cretaceous Laramide and Cenozoic tectonics in southeastern Arizona: Geological Society of America Bulletin, v. 133, p. 1996–2016, https://doi.org/10.1130/B35808.1.

Cecil, M.R., Rotberg, G.L., Ducea, M.N., Saleeby, J.B., and Gehrels, G.E., 2012, Magmatic growth and batholithic root development in the northern Sierra Nevada, California: Geosphere, v. 8, p. 592–606, https://doi.org/10.1130/GES00729.1.

Cerveny, P.F., III, 1990, Fission-track thermochronology of the Wind River Range and other basement-cored uplifts in the Rocky Mountain foreland [Ph.D. thesis]: Laramie, Wyoming, University of Wyoming, 189 p.

Cerveny, P.F., and Steidtmann, J.R., 1993, Fission track thermochronology of the Wind River Range, Wyoming: Evidence for timing and magnitude of Laramide exhumation: Tectonics, v. 12, p. 77–91, https://doi.org/10.1029/92TC01567.

Chapin, C.E., 2012, Origin of the Colorado Mineral Belt: Geosphere, v. 8, p. 28–43, https://doi.org/10.1130/GES00694.1.

Chapman, J.B., Runyon, S.E., Shields, J.E., Lawler, B.L., Pridmore, C.J., Scoggin, S.H., Swaim, N.T., Trzinski, A.E., Wiley, H.N., Barth, A.P., and Haxel, G.B., 2021, The North American Cordilleran Anatectic Belt: Earth-Science Reviews, v. 215, https://doi.org/10.1016/j.earscirev.2021.103576.

Chapman, J.B., Clinkscales, C., Trzinski, A., and Daniel, M., 2024, Evidence for a Late Cretaceous to Paleogene basement-involved retroarc wedge in the southern U.S. Cordillera: A case study from the northern Chiricahua Mountains, Arizona: Geological Society of America Bulletin, https://doi.org/10.1130/B37877.1.

Clinkscales, C., and Kapp, P., 2019, Structural style and kinematics of the Taihang-Luliangshan fold belt, North China: Implications for the Yanshanian orogeny: Lithosphere, v. 11, p. 767–783, https://doi.org/10.1130/L1096.1.

Coney, P.J., and Reynolds, S.J., 1977, Cordilleran Benioff zones: Nature, v. 270, p. 403–406, https://doi.org/10.1038/270403a0.

Constenius, K.N., Esser, R.P., and Layer, P.W., 2003, Extensional collapse of the Charleston-Nebo salient and its relationship to space-time variations in Cordilleran orogenic belt tectonism and continental stratigraphy, *in* Raynolds, R.G., and Flores, R.M., eds., Cenozoic Systems of the Rocky Mountain Region: Rocky Mountain Section Society for Sedimentary Geology (SEPM), p. 303–353.

Coogan, J.C., 1992, Structural evolution of piggyback basins in the Wyoming-Idaho-Utah thrust belt, *in* Link, P.K., Kuntz, M.A., and Piatt, L.B., eds., Regional Geology of Eastern Idaho and Western Wyoming: Geological Society of America Memoir 179, p. 55–82, https://doi.org/10.1130/MEM179-p55.

Copeland, P., Currie, C.A., Lawton, T.F., and Murphy, M.A., 2017, Location, location, location: The variable lifespan of the Laramide orogeny: Geology, v. 45, p. 223–226, https://doi.org/10.1130/G38810.1.

Crews, S.G., and Ethridge, F.G., 1993, Laramide tectonics and humid alluvial fan sedimentation, NE Uinta Uplift, Utah and Wyoming: Journal of Sedimentary Research, v. 63, no. 3, p. 420–436, https://doi.org/10.1306/D4267B18-2B26-11D7-8648000102C1865D.

Cross, T.A., 1986, Tectonic controls of foreland basin subsidence and Laramide style deformation, western United States, *in* Allen, P.A., and Homewood, P., eds., Foreland Basins: International Association of Sedimentologists Special Publication 8, p. 13–39, https://doi.org/10.1002/9781444303810.ch1.

Crowley, P.D., Reiners, P.W., Reuter, J.M., and Kaye, G.D., 2002, Laramide exhumation of the Bighorn Mountains, Wyoming: An apatite (U-Th)/He thermochronology study: Geology, v. 30, p. 27–30, https://doi.org/10.1130/0091-7613(2002)030<0027:LEOTBM>2.0.CO;2.

Currie, B.S., 2002, Structural configuration of the Early Cretaceous Cordilleran foreland-basin system and Sevier thrust belt, Utah and Colorado: The Journal of Geology, v. 110, p. 697–718, https://doi.org/10.1086/342626.

Davis, G.H., 1979, Laramide folding and faulting in southeastern Arizona: American Journal of Science, v. 279, p. 543–569, https://doi.org/10.2475/ajs.279.5.543.

Davis, G.H., Reeher, L.J., Jepson, G., Carrapa, B., DeCelles, P.G., and Chaudoir, K.M., 2022, Structure and thermochronology of basement/cover relations along the Defiance uplift (AZ and NM), and implications regarding Laramide tectonic evolution of the Colorado Plateau: American Journal of Science, v. 322, p. 1047–1087, https://doi.org/10.2475/09.2022.02.

Davis, G.H., et al., 2023, Structural Analysis and Chronologic Constraints on Progressive Deformation within the Rincon Mountains, Arizona: Implications for Development of Metamorphic Core Complexes: Geological Society of America Memoir 222, 125 p., https://doi.org/10.1130/2023.1222(01).

DeCelles, P.G., 1994, Late Cretaceous–Paleocene synorogenic sedimentation and kinematic history of the Sevier thrust belt, northeast Utah and southwest Wyoming: Geological Society of America Bulletin, v. 106, p. 32–56, https://doi.org/10.1130/0016-7606(1994)106<0032:LCPSSA>2.3.CO;2.

DeCelles, P.G., 2004, Late Jurassic to Eocene evolution of the Cordilleran thrust belt and foreland basin system, western USA: American Journal of Science, v. 304, p. 105–168, https://doi.org/10.2475/ajs.304.2.105.

DeCelles, P.G., and Coogan, J.C., 2006, Regional structure and kinematic history of the Sevier fold-and-thrust belt, central Utah: Geological Society of America Bulletin, v. 118, p. 841–864, https://doi.org/10.1130/B25759.1.

DeCelles, P.G., Tolson, R.B., Graham, S.A., Smith, G.A., Ingersoll, R.V., White, J., Schmidt, C.J., Rice, R., Moxon, I., Lemke, L., Handschy, J.W., Follo, M.F., Edwards, D.P., Cavazza, W., Caldwell, M., and Bargar, E., 1987, Laramide thrust-generated alluvial-fan sedimentation, Sphinx Conglomerate, southwestern Montana: AAPG Bulletin, v. 71, p. 135–155.

DeCelles, P.G., Gray, M.B., Ridgway, K.D., Cole, R.B., Pivnik, D.A., Pequera, N., and Srivastava, P., 1991a, Controls on synorogenic alluvial-fan architecture, Beartooth Conglomerate (Palaeocene), Wyoming and Montana: Sedimentology, v. 38, p. 567–590, https://doi.org/10.1111/j.1365-3091.1991.tb01009.x.

DeCelles, P.G., Gray, M.B., Ridgway, K.D., Cole, R.B., Srivastava, P., Pequera, N., and Pivnik, D.A., 1991b, Kinematic history of a foreland uplift from Paleocene synorogenic conglomerate, Beartooth Range, Wyoming and Montana: Geological Society of America Bulletin, v. 103, p. 1458–1475, https://doi.org/10.1130/0016-7606(1991)103<1458:KHOAFU>2.3.CO;2.

Devlin, W.J., Rudolph, K.W., Shaw, C.A., and Ehman, K.D., 1993, The effect of tectonic and eustatic cycles on accommodation and sequence-stratigraphic framework in the Upper Cretaceous foreland basin of southwestern Wyoming, *in* Posamentier, H.W., Summerhayes, C.P., Haq, B.U., and Allen, G.P., eds., Sequence Stratigraphy and Facies Associations: International Association of Sedimentologists Special Publication 18, p. 501–520, https://doi.org/10.1002/9781444304015.ch25.

Dickinson, W.R., and Snyder, W.S., 1978, Plate tectonics of the Laramide orogeny, *in* Matthews, V., III, ed., Laramide Folding Associated with Basement Block Faulting in the Western United States: Geological Society of America Memoir 151, p. 355–366, https://doi.org/10.1130/MEM151-p355.

Dickinson, W.R., Klute, M.A., Hayes, M.J., Janecke, S.U., Lundin, E.R., McKittrick, M.A., and Olivares, M.D., 1988, Paleogeographic and paleotectonic setting of Laramide sedimentary basins in the central Rocky Mountain region: Geological Society of America Bulletin, v. 100, p. 1023–1039, https://doi.org/10.1130/0016-7606(1988)100<1023:PAPSOL>2.3.CO;2.

Dickinson, W.R., Hopson, C.A., and Saleeby, J.B., 1996, Alternate origins of the Coast Range Ophiolite (California): Introduction and implications: GSA Today, v. 6, no. 2, p. 1–10, https://rock.geosociety.org/gsatoday/archive/6/2/pdf/i1052-5173-6-2-sci.pdf.

Di Fiori, R.V., Long, S.P., Fetrow, A.C., Snell, K.E., Bonde, J.W., and Vervoort, J.D., 2021, The role of shortening in the Sevier hinterland within the U.S. Cordilleran retroarc thrust system: Insights from the cretaceous Newark canyon formation in central Nevada: Tectonics, v. 40, https://doi.org/10.1029/2020TC006331.

Doelling, H.H., 2008, Geologic map of the Kanab 30′ × 60′ quadrangle, Kand and Washington Counties, Utah and Coconino and Mohave Counties, Arizona: Utah Geological Survey, scale 1:100,000, https://doi.org/10.34191/MP-08-2dm.

Donelick, R.A., O'Sullivan, P.B., and Ketcham, R.A., 2005, Apatite fission-track analysis: Reviews in Mineralogy and Geochemistry, v. 58, p. 49–94, https://doi.org/10.2138/rmg.2005.58.3.

Dorr, J.A., Spearing, D., and Steidtmann, J.R., 1977, Deformation and Deposition between a Foreland Uplift and an Impinging Thrust Belt: Hoback Basin, Wyoming: Geological Society of America Special Paper 177, 88 p., https://doi.org/10.1130/SPE177-p1.

Doubrovine, P.V., and Tarduno, J.A., 2008, A revised kinematic model for the relative motion between Pacific oceanic plates and North America since the Late Cretaceous: Journal of Geophysical Research: Solid Earth, v. 113, https://doi.org/10.1029/2008JB005585.

Ducea, M., 2001, The California arc: Thick granitic batholiths, eclogitic residues, lithospheric-scale thrusting, and magmatic flare-ups: GSA Today, v. 11, no. 11, p. 4–10, https://doi.org/10.1130/1052-5173(2001)011<0004:TCATGB>2.0.CO;2.

Ducea, M.N., and Barton, M.D., 2007, Igniting flare-up events in Cordilleran arcs: Geology, v. 35, p. 1047–1050, https://doi.org/10.1130/G23898A.1.

Ducea, M.N., and Saleeby, J.B., 1998, The age and origin of a thick mafic-ultramafic keel from beneath the Sierra Nevada batholith: Contributions to Mineralogy and Petrology, v. 133, p. 169–185, https://doi.org/10.1007/s004100050445.

Dumitru, T.A., 1990, Subnormal Cenozoic geothermal gradients in the extinct Sierra Nevada magmatic arc: Consequences of Laramide and post-Laramide shallow-angle subduction: Journal of Geophysical Research: Solid Earth, v. 95, p. 4925–4941, https://doi.org/10.1029/JB095iB04p04925

Dumitru, T.A., Duddy, I.R., and Green, P.F., 1994, Mesozoic-Cenozoic burial, uplift, and erosion history of the west-central Colorado Plateau: Geology, v. 22, p. 499–502, https://doi.org/10.1130/0091-7613(1994)022<0499:MCBUAE>2.3.CO;2.

Dunne, G.C., and Walker, J.D., 1993, Age of Jurassic volcanism and tectonism, southern Owens Valley region, east-central California: Geological Society of America Bulletin, v. 105, p. 1223–1230, https://doi.org/10.1130/0016-7606(1993)105<1223:AOJVAT>2.3.CO;2.

Economos, R.C., Barth, A.P., Wooden, J.L., Paterson, S.R., Friesenhahn, B., Wiegand, B.A., Anderson, J.L., Roell, J.L., Palmer, E.F., Ianno, A.J., and Howard, K.A., 2021, Testing models of Laramide orogenic initiation by investigation of Late Cretaceous magmatic-tectonic evolution of the central Mojave sector of the California arc: Geosphere, v. 17, p. 2042–2061, https://doi.org/10.1130/GES02225.1.

Engebretson, D.C., Cox, A., and Thompson, G.A., 1984, Correlation of plate motions with continental tectonics: Laramide to basin-range: Tectonics, v. 3, p. 115–119, https://doi.org/10.1029/TC003i002p00115.

Engebretson, D.C., Cox, A., and Gordon, R.G., 1985, Relative Motions between Oceanic and Continental Plates in the Pacific Basin: Geological Society of America Special Paper 206, 59 p., https://doi.org/10.1130/SPE206-p1.

Erslev, E.A., 1991, Trishear fault-propagation folding: Geology, v. 19, p. 617–620, https://doi.org/10.1130/0091-7613(1991)019<0617:TFPF>2.3.CO;2.

Erslev, E.A., 1993, Thrusts, back-thrusts and detachment of Rocky Mountain foreland arches, *in* Schmidt, C.J., Chase, R.B., and Erslev, E.A., eds., Laramide Basement Deformation in the Rocky Mountain Foreland of the Western United States: Geological Society of America Special Paper 280, p. 339–358, https://doi.org/10.1130/SPE280-p339.

Erslev, E.A., Worthington, L.L., Anderson, M.L., and Miller, K.C., 2022, Laramide crustal detachment in the Rockies: Cordilleran shortening of fluid-weakened foreland crust: Rocky Mountain Geology, v. 57, no. 2, p. 65–97, https://doi.org/10.24872/rmgjournal.57.2.65.

Fan, M., and Carrapa, B., 2014, Late Cretaceous–early Eocene Laramide uplift, exhumation, and basin subsidence in Wyoming: Crustal responses to flat slab subduction: Tectonics, v. 33, p. 509–529, https://doi.org/10.1002/2012TC003221.

Fan, M., Quade, J., Dettman, D., and DeCelles, P.G., 2011, Widespread basement erosion during the late Paleocene–early Eocene in the Laramide Rocky Mountains inferred from $^{87}Sr/^{86}Sr$ ratios of freshwater bivalve fossils: Geological Society of America Bulletin, v. 123, p. 2069–2082, https://doi.org/10.1130/B30219.1.

Farley, K.A., 2002, (U-Th)/He dating: Techniques, calibrations, and applications: Reviews in Mineralogy and Geochemistry, v. 47, p. 819–844, https://doi.org/10.2138/rmg.2002.47.18.

Favorito, D.A., and Seedorff, E., 2018, Discovery of major basement-cored uplifts in the northern Galiuro Mountains, Southeastern Arizona: Implications for regional Laramide deformation style and structural evolution: Tectonics, v. 37, p. 3916–3940, https://doi.org/10.1029/2018TC005180.

Feeley, T.C., 2003, Origin and tectonic implications of across-strike geochemical variations in the Eocene Absaroka volcanic province, United States: The Journal of Geology, v. 111, p. 329–346, https://doi.org/10.1086/373972.

Finn, T.M., and Johnson, R.C., 2005, Subsurface stratigraphic cross sections of Cretaceous and lower Tertiary rocks in the southwestern Wyoming Province, Wyoming, Colorado, and Utah, *in* Petroleum Systems and Geologic Assessment of Oil and Gas in the Southwestern Wyoming Province, Wyoming, Colorado, and Utah: U.S. Geological Survey, Digital Data Series, DDS-69-D, https://pubs.usgs.gov/dds/dds-069/dds-069-d/ [on CD-ROM].

Finzel, E.S., Rosenblume, J.A., Pearson, D.M., and Zippi, P.A., 2023, Timing of the transition from Sevier- to Laramide-style tectonism in southwestern Montana based on the provenance of the Frontier Formation, North American Cordillera: Tectonics, v. 42, https://doi.org/10.1029/2023TC007777.

Fitzgerald, P.G., Baldwin, S.L., Webb, L.E., and O'Sullivan, P.B., 2006, Interpretation of (U-Th)/He single grain ages from slowly cooled crustal terranes: A case study from the Transantarctic Mountains of southern Victoria Land: Chemical Geology, v. 225, p. 91–120, https://doi.org/10.1016/j.chemgeo.2005.09.001.

Flansburg, M.E., and Stockli, D.F., 2023, Progressive Miocene unroofing of the Big Maria and Riverside Mountains (southeastern California, USA) along the southwestern margin of the Colorado River extensional corridor: Geosphere, v. 19, p. 676–694, https://doi.org/10.1130/GES02564.1.

Fletcher, M., Wyman, D.A., and Zahirovic, S., 2020, Mantle plumes, triple junctions and transforms: A reinterpretation of Pacific Cretaceous–Tertiary LIPs and the Laramide connection: Geoscience Frontiers, v. 11, p. 1133–1144, https://doi.org/10.1016/j.gsf.2019.09.003.

Flowers, R.M., and Kelley, S.A., 2011, Interpreting data dispersion and "inverted" dates in apatite (U–Th)/He and fission-track datasets: An example from the US midcontinent: Geochimica et Cosmochimica Acta, v. 75, p. 5169–5186, https://doi.org/10.1016/j.gca.2011.06.016.

Flowers, R.M., Wernicke, B.P., and Farley, K.A., 2008, Unroofing, incision, and uplift history of the southwestern Colorado Plateau from apatite (U-Th)/He thermochronometry: Geological Society of America Bulletin, v. 120, p. 571–587, https://doi.org/10.1130/B26231.1.

Flowers, R.M., Ketcham, R.A., Shuster, D.L., and Farley, K.A., 2009, Apatite (UTh)/He thermochronometry using a radiation damage accumulation and annealing model: Geochimica et Cosmochimica Acta, v. 73, p. 2347–2365, https://doi.org/10.1016/j.gca.2009.01.015.

Flowers, R.M., Farley, K.A., and Ketcham, R.A., 2015, A reporting protocol for thermochronologic modeling illustrated with data from the Grand Canyon: Earth and Planetary Science Letters, v. 432, p. 425–435, https://doi.org/10.1016/j.epsl.2015.09.053.

Fowler, D.W., 2017, Revised geochronology, correlation, and dinosaur stratigraphic ranges of the Santonian-Maastrichtian (Late Cretaceous) formations of the Western Interior of North America: PLoS One, v. 12, https://doi.org/10.1371/journal.pone.0188426.

Galbraith, R.F., 2005, Statistics for Fission Track Analysis: CRC Press, 240 p., https://doi.org/10.1201/9781420034929.

Gallagher, K., 2012, Transdimensional inverse thermal history modeling for quantitative thermochronology: Journal of Geophysical Research: Solid Earth, v. 117, B2, https://doi.org/10.1029/2011JB008825.

Gehrels, G., Rusmore, M., Woodsworth, G., Crawford, M., Andronicos, C., Hollister, L., Patchett, J., Ducea, M., Butler, R., Klepeis, K., Davidson, C., Friedman, R., Haggart, J., Mahoney, B., Crawford, W., Pearson, D., and Girardi, J., 2009, U-Th-Pb geochronology of the Coast Mountains batholith in north-coastal British Columbia: Constraints on age and tectonic evolution: Geological Society of America Bulletin, v. 121, p. 1341–1361, https://doi.org/10.1130/B26404.1.

George, S.W., Perez, N.D., Struble, W., Curry, M.E., and Horton, B.K., 2022, Aseismic ridge subduction focused late Cenozoic exhumation above the Peruvian flat slab: Earth and Planetary Science Letters, v. 600, https://doi.org/10.1016/j.epsl.2022.117754.

Gerin, C., Gautheron, C., Oliviero, E., Bachelet, C., Mbongo Djimbi, D., Seydoux-Guillaume, A.-M., Tassan-Got, L.,

Sarda, P., Roques, J., and Garrido, F., 2017, Influence of vacancy damage on He diffusion in apatite, investigated at atomic to mineralogical scales: Geochimica et Cosmochimica Acta, v. 197, p. 87–103, https://doi.org/10.1016/j.gca.2016.10.018.

Giallorenzo, M.A., Wells, M.L., Yonkee, W.A., Stockli, D.F., and Wernicke, B.P., 2018, Timing of exhumation, Wheeler Pass thrust sheet, southern Nevada and California: Late Jurassic to middle Cretaceous evolution of the southern Sevier fold-and-thrust belt: Geological Society of America Bulletin, v. 130, p. 558–579, https://doi.org/10.1130/B31777.1.

Gleadow, A.J.W., Hurford, A.J., and Quaife, R.D., 1976, Fission track dating of zircon: Improved etching techniques: Earth and Planetary Science Letters, v. 33, p. 273–276, https://doi.org/10.1016/0012-821X(76)90235-1.

Gleadow, A.J.W., Duddy, I.R., Green, P.F., and Lovering, J.F., 1986, Confined fission track lengths in apatite: A diagnostic tool for thermal history analysis: Contributions to Mineralogy and Petrology, v. 94, p. 405–415, https://doi.org/10.1007/BF00376334.

Goldstrand, P.M., 1994, Tectonic development of Upper Cretaceous to Eocene strata of southwestern Utah: Geological Society of America Bulletin, v. 106, p. 145–154, https://doi.org/10.1130/0016-7606(1994)106<0145:TDOUCT>2.3.CO;2.

Gooley, J.T., Johnson, C.L., and Pettinga, L., 2016, Spatial and temporal variation of fluvial architecture in a prograding clastic wedge of the Late Cretaceous Western Interior Basin (Kaiparowits Plateau), USA: Journal of Sedimentary Research, v. 86, p. 125–147, https://doi.org/10.2110/jsr.2016.11.

Graham, S.A., Tolson, R.B., DeCelles, P.G., Ingersoll, R.V., Bargar, E., Caldwell, M., Cavazza, W., Edwards, D.P., Follo, M.F., Handschy, J.F., and Lemke, L., 1986, Provenance modelling as a technique for analysing source terrane evolution and controls on foreland sedimentation, *in* Allen, P.A., and Homewood, P., eds., Foreland Basins: Wiley, p. 425–436, https://doi.org/10.1002/9781444303810.ch23.

Greene, D.C., 2014, The Confusion Range, west-central Utah: Fold-thrust deformation and a western Utah thrust belt in the Sevier hinterland: Geosphere, v. 10, p. 148–169, https://doi.org/10.1130/GES00972.1.

Guo, H., Zeitler, P.K., Idleman, B.D., Fayon, A.K., Fitzgerald, P.G., and McDannell, K.T., 2021, Helium diffusion systematics inferred from continuous ramped heating analysis of Transantarctic Mountains apatites showing age overdispersion: Geochimica et Cosmochimica Acta, v. 310, p. 113–130, https://doi.org/10.1016/j.gca.2021.07.015.

Hackman, R.J., and Olson, A.B., 1977, Geology, structure, and uranium deposits of the Gallup 1 × 2 Quadrangle, New Mexico and Arizona: U.S. Geological Survey IMAP 981, scale 1:250,000, https://doi.org/10.3133/i981.

Hackman, R.J., and Wyant, D.G., 1973, Geology, structure, and uranium deposits of the Escalante Quadrangle, Utah and Arizona: U.S. Geological Survey IMAP 744, scale 1:250,000, https://doi.org/10.3133/i744.

Haley, J.C., 1986, Upper Cretaceous (Beaverhead) synorogenic sediments in the Montana-Idaho thrust belt and adjacent foreland: Relationships between sedimentation and tectonism [Ph.D. dissertation]: Baltimore, Maryland, The Johns Hopkins University, 542 p.

Hamilton, W., 1969, Mesozoic California and the underflow of Pacific mantle: Geological Society of America Bulletin, v. 80, p. 2409–2430, https://doi.org/10.1130/0016-7606(1969)80[2409:MCATUO]2.0.CO;2.

Harper, G.D., and Wright, J.E., 1984, Middle to late Jurassic tectonic evolution of the Klamath Mountains, California-Oregon: Tectonics, v. 3, p. 759–772, https://doi.org/10.1029/TC003i007p00759.

Haynes, D.D., Vogel, J.D., and Wyant, D.G., 1972, Geology, structure, and uranium deposits of the Cortez Quadrangle, Colorado and Utah: U.S. Geological Survey IMAP 629, scale 1:250,000, https://doi.org/10.3133/i629.

He, J., Thomson, S.N., Reiners, P.W., Hemming, S.R., and Licht, K.J., 2021, Rapid erosion of the Central Transantarctic Mountains at the Eocene-Oligocene transition: Evidence from skewed (U-Th)/He date distributions near Beardmore Glacier: Earth and Planetary Science Letters, v. 567, https://doi.org/10.1016/j.epsl.2021.117009.

Heller, P.L., and Liu, L., 2016, Dynamic topography and vertical motion of the U.S. Rocky Mountain region prior to and during the Laramide orogeny: Geological Society of America Bulletin, v. 128, p. 973–988, https://doi.org/10.1130/B31431.1.

Henderson, L.J., Gordon, R.G., and Engebretson, D.C., 1984, Mesozoic aseismic ridges on the Farallon plate and southward migration of shallow subduction during the Laramide orogeny: Tectonics, v. 3, p. 121–132, https://doi.org/10.1029/TC003i002p00121.

Hoppin, R.A., 1961, Precambrian rocks and their relationship to Laramide structure along the east flank of the Bighorn Mountains near Buffalo, Wyoming: Geological Society of America Bulletin, v. 72, p. 351–367, https://doi.org/10.1130/0016-7606(1961)72[351:PRATRT]2.0.CO;2.

Howlett, C.J., Reynolds, A.N., and Laskowski, A.K., 2021, Magmatism and extension in the Anaconda Metamorphic Core Complex of western Montana and relation to regional tectonics: Tectonics, v. 40, https://doi.org/10.1029/2020TC006431.

Howlett, C.J., Jepson, G., Carrapa, B., DeCelles, P.G., and Constenius, K.N., 2024, Late Cretaceous exhumation of the Little Belt Mountains and regional development of the Helena salient, west-central Montana, USA: Geological Society of America Bulletin, v. 136, p. 2256–2280, https://doi.org/10.1130/B37081.1.

Hoy, R.G., and Ridgway, K.D., 1997, Structural and sedimentological development of footwall growth synclines along an intraforeland uplift, east-central Bighorn Mountains, Wyoming: Geological Society of America Bulletin, v. 109, p. 915–935, https://doi.org/10.1130/0016-7606(1997)109<0915:SASDOF>2.3.CO;2.

Hurford, A.J., and Green, P.F., 1983, The zeta age calibration of fission-track dating: Chemical Geology, v. 41, p. 285–317, https://doi.org/10.1016/S0009-2541(83)80026-6.

Jacobson, C.E., Grove, M., Pedrick, J.N., Barth, A.P., Marsaglia, K.M., Gehrels, G.E., and Nourse, J.A., 2011, Late Cretaceous–early Cenozoic tectonic evolution of the southern California margin inferred from provenance of trench and forearc sediments: Geological Society of America Bulletin, v. 123, p. 485–506, https://doi.org/10.1130/B30238.1.

Jamison, W.R., and Stearns, D.W., 1982, Tectonic deformation of Wingate Sandstone, Colorado National Monument: AAPG Bulletin, v. 66, p. 2584–2608, https://doi.org/10.1306/03B5AC7D-16D1-11D7-8645000102C1865D.

Jepson, G., Carrapa, B., George, S.W., Triantafyllou, A., Egan, S.M., Constenius, K.N., Gehrels, G.E., and Ducea, M.N., 2021, Resolving mid-to upper-crustal exhumation through apatite petrochronology and thermochronology: Chemical Geology, v. 565, https://doi.org/10.1016/j.chemgeo.2021.120071.

Jepson, G., et al., 2022, Where did the Arizona-Plano go?: Protracted thinning via upper-to lower-crustal processes: Journal of Geophysical Research: Solid Earth, v. 127, https://doi.org/10.1029/2021JB023850.

Jones, C.H., Farmer, G.L., Sageman, B., and Zhong, S., 2011, Hydrodynamic mechanism for the Laramide orogeny: Geosphere, v. 7, p. 183–201, https://doi.org/10.1130/GES00575.1.

Jordan, T.E., 1981, Thrust loads and foreland basin evolution, Cretaceous, western United States: AAPG Bulletin, v. 65, p. 2506–2520, https://doi.org/10.1306/03B599F4-16D1-11D7-8645000102C1865D.

Jordan, T.E., and Allmendinger, R.W., 1986, The Sierras Pampeanas of Argentina; a modern analogue of Rocky Mountain foreland deformation: American Journal of Science, v. 286, p. 737–764, https://doi.org/10.2475/ajs.286.10.737.

Kapp, P., Jepson, G., Carrapa, B., Schaen, A.J., He, J.J., and Wang, J.W., 2023, Laramide bulldozing of lithosphere beneath the Arizona transition zone, southwestern United States: Geology, v. 51, p. 952–956, https://doi.org/10.1130/G51194.1.

Karlstrom, K.E., Crossey, L.J., Embid, E., Crow, R., Heizler, M., Hereford, R., Beard, L.S., Ricketts, J.W., Cather, S., and Kelley, S., 2017, Cenozoic incision history of the Little Colorado River: Its role in carving Grand Canyon and onset of rapid incision in the past ca. 2 Ma in the Colorado River: Geosphere, v. 13, p. 49–81, https://doi.org/10.1130/GES01304.1.

Karlstrom, K.E., Wilgus, J., Thacker, J.O., Schmandt, B., Coblentz, D., and Albonico, M., 2022, Tectonics of the Colorado Plateau and its margins: Annual Review of Earth and Planetary Sciences, v. 50, p. 295–322, https://doi.org/10.1146/annurev-earth-032320-111432.

Kauffman, E.G., 1985, Cretaceous evolution of the Western Interior Basin of the United States, *in* Pratt, L.M., Kauffman, E.G., and Zelt, F.B., eds., Fine-Grained Deposits and Biofacies of the Cretaceous Western Interior Seaway: Evidence of Cyclic Sedimentary Processes: Society for Sedimentary Geology (SEPM) Geology Field Trip Guidebook 4, Midyear Meeting, Golden, Colorado, p. IV–XI, https://doi.org/10.2110/sepmfg.04.

Kauffman, E.G., and Caldwell, W.G.E., 1993, The Western Interior Basin in space and time, *in* Caldwell, WG.E., and Kauffman, E.G., eds., Evolution of the Western Interior Basin: Geological Association of Canada Special Paper 39, p. 1–30.

Keefer, W.R., 1970, Structural geology of the Wind River basin, Wyoming: U.S. Geological Survey Professional Paper 495-D, 35 p., https://doi.org/10.3133/pp495D.

Kelley, S.A., 2005, Low-temperature cooling histories of the Cheyenne Belt and Laramie Peak Shear Zone, Wyoming, and the Soda Creek–Fish Creek Shear Zone, Colorado: American Geophysical Union, p. 55–70, https://doi.org/10.1029/154GM05.

Kelley, S.A., and Chapin, C.E., 1997, Cooling histories of mountain ranges in the southern Rio Grande rift based on apatite fission-track analysis—A reconnaissance survey: New Mexico Geology, v. 19, no. 1, p. 1–14, https://doi.org/10.58799/NMG-v19n1.1.

Kelley, S.A., and Chapin, C.E., 2004, Denudational histories of the Front Range and Wet Mountains, Colorado, based on apatite fission-track thermochronology, *in* Cather, S.M., McIntosh, W., and Kelley, S.A., eds., Tectonics, Geochronology and Volcanism in the Southern Rocky Mountains and Rio Grande Rift: New Mexico Bureau of Geology and Mineral Resources Bulletin 160, p. 41–77.

Kelley, S.A., and Duncan, I.J., 1986, Late Cretaceous to middle Tertiary tectonic history of the northern Rio Grande rift, New Mexico: Journal of Geophysical Research: Solid Earth, v. 91, B6, p. 6246–6262, https://doi.org/10.1029/JB091iB06p06246.

Kelley, S.A., and Karlstrom, K.E., 2012, The Laramide and post-Laramide uplift and erosional history of the eastern Grand Canyon: Evidence from apatite fission-track thermochronology, *in* Timmons, J.M., and Karlstrom, K.E., eds., Grand Canyon Geology: Two Billion Years of Earth's History: Geological Society of America Special Paper 489, p. 109–118, https://doi.org/10.1130/2012.2489(07).

Kelley, S.A., Chapin, C.E., and Corrigan, J., 1992, Late Mesozoic to Cenozoic cooling histories of the flanks of the northern and central Rio Grande rift, Colorado and New Mexico: New Mexico Bureau of Mines and Mineral Resources, Bulletin 145, 39 p., https://doi.org/10.58799/B-145.

Kelley, S.A., Chapin, C.E., Karlstrom, K.E., Young, R.A., and Spamer, E.E., 2001, Laramide cooling histories of Grand Canyon, Arizona, and the Front Range, Colorado, determined from apatite fission-track thermochronology, *in* Young, R.A., and Spamer, E.E., eds., Colorado River Origin and Evolution: Grand Canyon National Park, Grand Canyon, Arizona: Grand Canyon Association, p. 37–42.

Kelley, V.C., 1967, Tectonics of the Zuni-Defiance region, New Mexico and Arizona, *in* Trauger, F.D., ed., Defiance-Zuni-Mt. Taylor region, Arizona and New Mexico: New Mexico Geological Society, Guidebook, 18th Field Conference, p. 28–31, https://doi.org/10.56577/FFC-18.28.

Ketcham, R.A., Carter, A., Donelick, R.A., Barbarand, J., and Hurford, A.J., 2007, Improved modeling of fission-track annealing in apatite: American Mineralogist, v. 92, p. 799, https://doi.org/10.2138/am.2007.2281.

Lamerson, P.R., 1982, The Fossil Basin and its relationship to the Absaroka thrust system, Wyoming and Utah: Rocky Mountain Association of Geologists, Geologic Studies of the Cordilleran Thrust Belt, v. 1, p. 279–340.

Laslett, G.M., Green, P.F., Duddy, I.R., and Gleadow, A.J.W., 1987, Thermal annealing of fission tracks in apatite: 2. A quantitative analysis: Chemical Geology, Isotope

Geoscience Section, v. 65, p. 1–13, https://doi.org/10.1016/0168-9622(87)90057-1.

Lawton, T.F., 1986, Fluvial systems of the Upper Cretaceous Mesaverde Group and Paleocene North Horn Formation, Central Utah: A record of transition from thin-skinned to thick-skinned deformation in the foreland region, *in* Peterson, J.A., ed., Paleotectonics and sedimentation in the Rocky Mountain Region, United States: American Association of Petroleum Geologists Memoir 41, p. 423–442, https://doi.org/10.1306/M41456C20.

Lawton, T.F., 2019, Laramide sedimentary basins and sediment-dispersal systems, *in* Miall, A.D., ed., The Sedimentary Basins of the United States and Canada: Elsevier, Sedimentary Basins of the World, v. 5, p. 529–557, https://doi.org/10.1016/B978-0-444-63895-3.00013-9.

Lawton, T.F., Boyer, S.E., and Schmitt, J.G., 1994, Influence of inherited taper on structural variability and conglomerate distribution, Cordilleran fold and thrust belt, western United States: Geology, v. 22, p. 339–342, https://doi.org/10.1130/0091-7613(1994)022<0339:IOITOS>2.3.CO;2.

Leary, R., DeCelles, P., Gehrels, G., and Morriss, M., 2015, Fluvial deposition during transition from flexural to dynamic subsidence in the Cordilleran foreland basin: Ericson Formation, Western Wyoming, USA: Basin Research, v. 27, p. 495–516, https://doi.org/10.1111/bre.12085.

Leckie, R.M., Schmidt, M.G., Finkelstein, D., and Yuretich, R., 1991, Paleoceanographic and paleoclimatic interpretations of the Mancos Shale (Upper Cretaceous), Black Mesa Basin, Arizona, *in* Nations, J.D., and Eaton, J.G., eds., Stratigraphy, depositional environments; and sedimentary tectonics of the western margin, Cretaceous Western Interior Seaway: Geological Society of America Special Paper 260, p. 139–152, https://doi.org/10.1130/SPE260-p139.

Levander, A., Schmandt, B., Miller, M.S., Liu, K., Karlstrom, K.E., Crow, R.S., Lee, C.T., and Humphreys, E.D., 2011, Continuing Colorado Plateau uplift by delamination-style convective lithospheric downwelling: Nature, v. 472, p. 461–465, https://doi.org/10.1038/nature10001.

Lisenbee, A.L., 1988, Tectonic history of the Black Hills uplift, *in* Diedrich, R.P., Dyka, M.A.K., and Miller, W.R., eds., Eastern Powder River Basin—Black Hills: Casper, Wyoming, Wyoming Geological Association, 39th Annual Field Conference, Guidebook, p. 45–52.

Liu, L., Gurnis, M., Seton, M., Saleeby, J., Müller, D.R., and Jackson, J.M., 2010, The role of oceanic plateau subduction in the Laramide orogeny: Nature Geoscience, v. 3, p. 353–357, https://doi.org/10.1038/ngeo829.

Liu, S., and Currie, C.A., 2016, Farallon plate dynamics prior to the Laramide orogeny: Numerical models of flat subduction: Tectonophysics, v. 666, p. 33–47, https://doi.org/10.1016/j.tecto.2015.10.010.

Liu, S., Nummedal, D., and Liu, L., 2011, Migration of dynamic subsidence across the Late Cretaceous United States Western Interior Basin in response to Farallon plate subduction: Geology, v. 39, p. 555–558, https://doi.org/10.1130/G31692.1.

Livaccari, R.F., 1991, Role of crustal thickening and extensional collapse in the tectonic evolution of the Sevier-Laramide orogeny, western United States: Geology, v. 19, p. 1104–1107, https://doi.org/10.1130/0091-7613(1991)019<1104:ROCTAE>2.3.CO;2.

Livaccari, R.F., Burke, K., and Şengör, A.M.C., 1981, Was the Laramide orogeny related to subduction of an oceanic plateau?: Nature, v. 289, p. 276–278, https://doi.org/10.1038/289276a0.

Long, S.P., 2012, Magnitudes and spatial patterns of erosional exhumation in the Sevier hinterland, eastern Nevada and western Utah, USA: Insights from a Paleogene paleogeologic map: Geosphere, v. 8, p. 881–901, https://doi.org/10.1130/GES00783.1.

Long, S.P., 2015, An upper-crustal fold province in the hinterland of the Sevier orogenic belt, eastern Nevada, USA: A Cordilleran Valley and Ridge in the Basin and Range: Geosphere, v. 11, p. 404–424, https://doi.org/10.1130/GES01102.1.

Long, S.P., Henry, C.D., Muntean, J.L., Edmondo, G.P., and Cassel, E.J., 2014, Early Cretaceous construction of a structural culmination, Eureka, Nevada, USA: Implications for out-of-sequence deformation in the Sevier hinterland: Geosphere, v. 10, p. 564–584, https://doi.org/10.1130/GES00997.1.

Love, J.D., and Christiansen, A.C., 1985, Geologic map of Wyoming: U.S. Geological Survey, 3 pl., scale 1:500,000, https://doi.org/10.3133/70210886.

Lowry, A.R., and Smith, R.B., 1995, Strength and rheology of the western US Cordillera: Journal of Geophysical Research: Solid Earth, v. 100, p. 17,947–17,963, https://doi.org/10.1029/95JB00747.

Marshak, S., Domrois, S., Abert, C., Larson, T., Pavlis, G., Hamburger, M., Yang, X., Gilbert, H., and Chen, C., 2017, The basement revealed: Tectonic insight from a digital elevation model of the Great Unconformity, USA cratonic platform: Geology, v. 45, p. 391–394, https://doi.org/10.1130/G38875.1.

Matthews, K.J., Seton, M., and Müller, R.D., 2012, A global-scale plate reorganization event at 105–100 Ma: Earth and Planetary Science Letters, v. 355–356, p. 283–298, https://doi.org/10.1016/j.epsl.2012.08.023.

May, S.R., Gray, G.G., Summa, L.L., Stewart, N.R., Gehrels, G.E., and Pecha, M.E., 2013, Detrital zircon geochronology from Cenomanian–Coniacian strata in the Bighorn Basin, Wyoming, USA: Implications for stratigraphic correlation and paleogeography: Rocky Mountain Geology, v. 48, p. 41–61, https://doi.org/10.2113/gsrocky.48.1.41.

McDowell, F.W., McIntosh, W.C., and Farley, K.A., 2005, A precise ^{40}Ar-^{39}Ar reference age for the Durango apatite (UTh)/He and fission-track dating standard: Chemical Geology, v. 214, p. 249–263, https://doi.org/10.1016/j.chemgeo.2004.10.002.

McGrew, A.J., Peters, M.T., and Wright, J.E., 2000, Thermobarometric constraints on the tectonothermal evolution of the East Humboldt Range metamorphic core complex, Nevada: Geological Society of America Bulletin, v. 112, p. 45–60, https://doi.org/10.1130/0016-7606(2000)112<45:TCOTTE>2.0.CO;2.

Mederos, S., Tikoff, B., and Bankey, V., 2005, Geometry, timing, and continuity of the Rock Springs uplift, Wyoming, and Douglas Creek arch, Colorado: Implications for uplift mechanisms in the Rocky Mountain foreland, USA: Rocky Mountain Geology, v. 40, p. 167–191, https://doi.org/10.2113/40.2.167.

Miall, A.D., Catuneanu, O., Vakarelov, B.K., and Post, R., 2008, The Western interior basin, *in* Miall, A.D., ed., The Sedimentary Basins of the United States and Canada: Elsevier, Sedimentary Basins of the World, v. 5, p. 329–362, https://doi.org/10.1016/S1874-5997(08)00009-9.

Miller, C.F., and Bradfish, L.J., 1980, An inner Cordilleran belt of muscovite-bearing plutons: Geology, v. 8, p. 412–416, https://doi.org/10.1130/0091-7613(1980)8<412:AICBOM>2.0.CO;2.

Miller, E.L., and Gans, P.B., 1989, Cretaceous crustal structure and metamorphism in the hinterland of the Sevier thrust belt, western US Cordillera: Geology, v. 17, p. 59–62, https://doi.org/10.1130/0091-7613(1989)017<0059:CCSAMI>2.3.CO;2.

Miller, E.L., Gans, P.B., Wright, J.E., Sutter, J.F., and Ernst, W.G., 1988, Metamorphic history of the east-central Basin and Range province: Tectonic setting and relationship to magmatism, *in* Ernst, W.G., ed., Metamorphism and Crustal Evolution, Western Conterminous United States: Englewood Cliffs, New Jersey, Prentice-Hall, Rubey Volume 7, p. 649–682.

Mitra, G., 1997, Evolution of salients in a fold-and-thrust belt: The effects of sedimentary basin geometry, strain distribution and critical taper, *in* Sengupta, S., ed., Evolution of Geological Structures in Micro- to Macro-Scales: London, Chapman and Hall, p. 59–90, https://doi.org/10.1007/978-94-011-5870-1_5.

Mitrovica, J.X., Beaumont, C., and Jarvis, G.T., 1989, Tilting of continental interiors by the dynamical effects of subduction: Tectonics, v. 8, p. 1079–1094, https://doi.org/10.1029/TC008i005p01079.

Mulcahy S.R., Starnes J.K., Day H.W., Coble M.A., Vervoort J.D., 2018, Early onset of Franciscan subduction: Tectonics, v. 37, p. 1194–1209, https://doi.org/10.1029/2017TC004753.

Müller, R.D., Seton, M., Zahirovic, S., Williams, S.E., Matthews, K.J., Wright, N.M., Shephard, G.E., Maloney, K.T., Barnett-Moore, N., Hosseinpour, M., Bower, D.J., and Cannon, J., 2016, Ocean basin evolution and global-scale plate reorganization events since Pangea breakup: Annual Reviews Earth and Planetary Science, v. 44, p. 107–138, https://doi.org/10.1146/annurev-earth-060115-012211.

Murray, K.E., Reiners, P.W., Thomson, S.N., Robert, X., and Whipple, K.X., 2019, The thermochronologic record of erosion and magmatism in the Canyonlands region of the Colorado Plateau: American Journal of Science, v. 319, p. 339–380, https://doi.org/10.2475/05.2019.01.

Naeser, C., Bryant, B., Kunk, M.J., Kellogg, K.S., Donelick, R., and Perry, W., Jr., 2002, Tertiary cooling and tectonic history of the White River uplift, Gore Range, and western Front Range, central Colorado: Evidence from fission-track and $^{39}Ar/^{40}Ar$ ages, *in* Kirkham, R.M., Scott, R.B., and Judkins, T.W., eds., Late Cenozoic Evaporite Tectonism and Volcanism in West-Central Colorado: Geological Society of America Special Paper 366, p. 31–53, https://doi.org/10.1130/0-8137-2366-3.31.

Naeser, N.D., 1992, Miocene cooling in the southwestern Powder River Basin, Wyoming: Preliminary evidence from apatite fission-track analysis: U.S. Geological Survey Bulletin 1917-O, 17 p., https://doi.org/10.3133/b1917O.

Neely, T.G., and Erslev, E.A., 2009, The interplay of fold mechanisms and basement weaknesses at the transition between Laramide basement-involved arches, north-central Wyoming, USA: Journal of Structural Geology, v. 31, p. 1012–1027, https://doi.org/10.1016/j.jsg.2009.03.008.

Nichols, D.J., Perry, W.J., Jr., and Haley Johns, J.C., 1985, Reinterpretation of the palynology and age of Laramide syntectonic deposits, southwestern Montana, and revision of the Beaverhead Group: Geology, v. 13, p. 149–153, https://doi.org/10.1130/0091-7613(1985)13<149:ROTPAA>2.0.CO;2.

Oldow, J.S., Bally, A.W., Avé Lallemant, H.G., and Leeman, W.P., 1989, Phanerozoic evolution of the North American Cordillera; United States and Canada, *in* Bally, A.W., and Palmer, A.R., eds., The Geology of North America—An Overview: Geological Society of America, Decade of North American Geology, Geology of North America, v. A, p. 139–232, https://doi.org/10.1130/DNAG-GNA-A.139.

Omar, G.I., Lutz, T.M., and Giegengack, R., 1994, Apatite fission-track evidence for Laramide and post-Laramide uplift and anomalous thermal regime at the Beartooth overthrust, Montana-Wyoming: Geological Society of America Bulletin, v. 106, p. 74–85, https://doi.org/10.1130/0016-7606(1994)106<0074:AFTEFL>2.3.CO;2.

O'Sullivan, R.B., and Beikman, H.M., 1963, Geology, structure, and uranium deposits of the Shiprock Quadrangle, New Mexico and Arizona: U.S. Geological Survey IMAP 345, 2 sheets, scale 1:250,000, https://doi.org/10.3133/i345.

Painter, C.S., and Carrapa, B., 2013, Flexural versus dynamic processes of subsidence in the North American Cordillera foreland basin: Geophysical Research Letters, v. 40, p. 4249–4253, https://doi.org/10.1002/grl.50831.

Painter, C.S., Carrapa, B., DeCelles, P.G., Gehrels, G.E., and Thomson, S.N., 2014, Exhumation of the North American Cordillera revealed by multi-dating of Upper Jurassic–Upper Cretaceous foreland basin deposits: Geological Society of America Bulletin, v. 126, p. 1439–1464, https://doi.org/10.1130/B30999.1.

Pang, M., and Nummedal, D., 1995, Flexural subsidence and basement tectonics of the Cretaceous Western Interior basin, United States: Geology, v. 23, p. 173–176, https://doi.org/10.1130/0091-7613(1995)023<0173:FSABTO>2.3.CO;2.

Parker, S.D., and Pearson, D.M., 2021, Pre-thrusting stratigraphic control on the transition from a thin-skinned to thick-skinned structural style: An example from the double-decker Idaho-Montana fold-thrust belt: Tectonics, v. 40, https://doi.org/10.1029/2020TC006429.

Paterson, S.R., Okaya, D., Memeti, V., Economos, R., and Miller, R.B., 2011, Magma addition and flux calculations of incrementally constructed magma chambers in continental margin arcs: Combined field, geochrono-

logic, and thermal modeling studies: Geosphere, v. 7, p. 1439–1468, https://doi.org/10.1130/GES00696.1.

Paylor, E.D., II, and Yin, A., 1993, Left-slip evolution of the North Owl Creek fault system, Wyoming, during Laramide shortening, *in* Schmidt, C.J., Chase, R.B., and Erslev, E.A., eds., Laramide Basement Deformation in the Rocky Mountain Foreland of the Western United States: Geological Society of America Special Paper 280, p. 229–242, https://doi.org/10.1130/SPE280-p229.

Peyton, L.S., and Carrapa, B., 2013, An overview of low-temperature thermochronology in the Rocky Mountains and its application to petroleum system analysis, *in* Knight, C., and Cuzella, J., eds., Application of Structural Methods to Rocky Mountain hydrocarbon exploration and development: American Association of Petroleum Geologists and Rocky Mountain Association of Geologists, AAPG Studies in Geology, v. 6, p. 37–70, https://doi.org/10.1306/13381689St653578.

Peyton, S.L., Reiners, P.W., Carrapa, B., and DeCelles, P.G., 2012, Low-temperature thermochronology of the northern Rocky Mountains, western U.S.A.: American Journal of Science, v. 312, p. 145–212, https://doi.org/10.2475/02.2012.04.

Premo, W.R., Morton, D.M., Wooden, J.L., Fanning, C.M., and Miller, F.K., 2014, U-Pb zircon geochronology of plutonism in the northern Peninsular Ranges batholith, southern California: Implications for the Late Cretaceous tectonic evolution of southern California, *in* Morton, D.M., and Miller, F.K., eds., Peninsular Ranges Batholith, Baja California and Southern California: Geological Society of America Memoir 211, p. 145–180, https://doi.org/10.1130/2014.1211(04).

Rautela, O., Chapman, A.D., Shields, J.E., Ducea, M.N., Lee, C.T., Jiang, H., and Saleeby, J., 2020, In search for the missing arc root of the Southern California Batholith: PTt evolution of upper mantle xenoliths of the Colorado Plateau Transition Zone: Earth and Planetary Science Letters, v. 547, https://doi.org/10.1016/j.epsl.2020.116447.

Redden, J.A., and DeWitt, E., 2008, Maps showing geology, structure, and geophysics of the central Black Hills, South Dakota: U.S. Geological Survey Scientific Investigations Map 2777, 2 sheets, scale 1:100,000, https://doi.org/10.3133/sim2777.

Reiners, P.W., 2005, Zircon (U-Th)/He thermochronometry: Reviews in Mineralogy and Geochemistry, v. 58, p. 151–179, https://doi.org/10.2138/rmg.2005.58.6.

Reiners, P.W., 2009, Nonmonotonic thermal histories and contrasting kinetics of multiple thermochronometers: Geochimica et Cosmochimica Acta, v. 73, p. 3612–3629, https://doi.org/10.1016/j.gca.2009.03.038.

Reiners, P.W., and Brandon, M.T., 2006, Using thermochronology to understand orogenic erosion: Annual Review of Earth and Planetary Sciences, v. 34, p. 419–466, https://doi.org/10.1146/annurev.earth.34.031405.125202.

Reiners, P.W., and Farley, K.A., 2001, Influence of crystal size on apatite (U-Th)/He thermochronology: An example from the Bighorn Mountains, Wyoming: Earth and Planetary Science Letters, v. 188, p. 413–420, https://doi.org/10.1016/S0012-821X(01)00341-7.

Roberts, S.V., and Burbank, D.W., 1993, Uplift and thermal history of the Teton Range (northwestern Wyoming) defined by apatite fission-track dating: Earth and Planetary Science Letters, v. 118, p. 295–309, https://doi.org/10.1016/0012-821X(93)90174-8.

Roehler, H.W., 1993, Eocene climates, depositional environments, and geography, greater Green River Basin, Wyoming, Utah, and Colorado: U.S. Geological Survey Professional Paper 1506-F, 74 p., https://doi.org/10.3133/pp1506F

Ronemus, C.B., Orme, D.A., Guenthner, W.R., Cox, S.E., and Kussmaul, C.A.L., 2023, Orogens of Big Sky Country: Reconstructing the deep-time tectonothermal history of the Beartooth Mountains, Montana and Wyoming, USA: Tectonics, v. 42, https://doi.org/10.1029/2022TC007541.

Rønnevik, C., Ksienzyk, A.K., Fossen, H., and Jacobs, J., 2017, Thermal evolution and exhumation history of the Uncompahgre Plateau (northeastern Colorado Plateau), based on apatite fission track and (U-Th)-He thermochronology and zircon U-Pb dating: Geosphere, v. 13, p. 518–537, https://doi.org/10.1130/GES01415.1.

Royse, E., Jr., Warner, M.A., and Reese, D.L., 1975, Thrust belt structural geometry and related stratigraphic problems, Wyoming, Idaho and northern Utah, *in* Bolyard, D.W., ed., Deep Drilling Frontiers of the Central Rocky Mountains: Rocky Mountain Association of Geologists Guidebook, p. 41–54.

Saleeby, J., 2003, Segmentation of the Laramide Slab evidence from the southern Sierra Nevada region: Geological Society of America Bulletin, v. 115, p. 655–668, https://doi.org/10.1130/0016-7606(2003)115<0655:SOTLSF>2.0.CO;2.

Saleeby, J.B., 1992, Petrotectonic and paleogeographic settings of U.S. Cordilleran ophiolites, *in* Burchfiel, B.C., Lipman, P.W., and Zoback, M.L., eds., The Cordilleran Orogen: Conterminous U.S.: Geological Society of America, Decade of North American Geology, Geology of North America, v. G-3, p. 653–682, https://doi.org/10.1130/DNAG-GNA-G3.653.

Saleeby, J.B., and Busby-Spera, C., 1992, Early Mesozoic tectonic evolution of the western U.S. Cordillera, *in* Burchfiel, B.C., Lipman, P.W., and Zoback, M.L., eds., The Cordilleran Orogen: Conterminous U.S.: Geological Society of America, Decade of North American Geology, Geology of North America, v. G-3, p. 107–138, https://doi.org/10.1130/DNAG-GNA-G3.107.

Saleeby, J.B., Busby-Spera, C., Oldow, J.S., Dunne, G.C., Wright, J.E., Cowan, D.S., Walker, N.W., and Allmendinger, R.W., 1992, Early Mesozoic tectonic evolution of the western U.S. Cordillera, *in* Burchfiel, B.C., Lipman, P.W., and Zoback, M.L., eds., The Cordilleran Orogen: Conterminous U.S.: Geological Society of America, Decade of North American Geology, Geology of North America, v. G-3, p. 139–168, https://doi.org/10.1130/DNAG-GNA-G3.107.

Sano, T., Hanyu, T., Tejada, M.L.G., Koppers, A.A., Shimizu, S., Miyazaki, T., Chang, Q., Senda, R., Vaglarov, B.S., Ueki, K., and Toyama, C., 2020, Two-stages of plume tail volcanism formed Ojin Rise Seamounts adjoining Shatsky Rise: Lithos, v. 372–373, https://doi.org/10.1016/j.lithos.2020.105652.

Saylor, J.E., Rudolph, K.W., Sundell, K.E., and van Wijk, J., 2020, Laramide orogenesis driven by Late Cretaceous weakening of the North American lithosphere: Journal of Geophysical Research: Solid Earth, v. 125, https://doi.org/10.1029/2020JB019570.

Schildgen, T.F., van der Beek, P.A., Sinclair, H.D., and Thiede, R.C., 2018, Spatial correlation bias in late-Cenozoic erosion histories derived from thermochronology: Nature, v. 559, p. 89–93, https://doi.org/10.1038/s41586-018-0260-6.

Schmidt, C.J., and Garihan, J.M., 1983, Laramide tectonic development of the Rocky Mountain foreland of southwestern Montana, *in* Lowell, J.D., and Gries, R., eds., Rocky Mountain Foreland Basins and Uplifts: Rocky Mountain Association of Geologists, p. 271–294.

Schmidt, C.J., O'Neill, J.M., and Brandon, W.C., 1988, Influence of Rocky Mountain foreland uplifts on the development of the frontal fold and thrust belt, southwestern Montana, *in* Schmidt, C.J., and Perry, W.J., Jr., eds., Interaction of the Rocky Mountain Foreland and the Cordilleran Thrust Belt: Geological Society of America Memoir 171, p. 171–202, https://doi.org/10.1130/MEM171-p171.

Schwartz, J.J., Lackey, J.S., Miranda, E.A., Klepeis, K.A., Mora-Klepeis, G., Robles, F., and Bixler, J.D., 2023, Magmatic surge requires two-stage model for the Laramide orogeny: Nature Communications, v. 14, https://doi.org/10.1038/s41467-023-39473-7.

Schwartz, T.M., Surpless, K.D., Colgan, J.P., Johnstone, S.A., and Holm-Denoma, C.S., 2021, Detrital zircon record of magmatism and sediment dispersal across the North American Cordilleran arc system (28–48°N): Earth-Science Reviews, v. 220, https://doi.org/10.1016/j.earscirev.2021.103734.

Shanley, K.W., and McCabe, P.J., 1991, Predicting facies architecture through sequence stratigraphy, an example from the Kaiparowits Plateau: Utah Geology, v. 19, p. 742–745, https://doi.org/10.1130/0091-7613(1991)019<0742:PFATSS>2.3.CO;2.

Shuster, D.L., Flowers, R.M., and Farley, K.A., 2006, The influence of natural radiation damage on helium diffusion kinetics in apatite: Earth and Planetary Science Letters, v. 249, p. 148–161, https://doi.org/10.1016/j.epsl.2006.07.028.

Smith, D., Connelly, J.N., Manser, K., Moser, D.E., Housh, T.B., McDowell, F.W., and Mack, L.E., 2004, Evolution of Navajo eclogites and hydration of the mantle wedge below the Colorado Plateau, southwestern United States: Geochemistry, Geophysics, Geosystems, v. 5, https://doi.org/10.1029/2003GC000675.

Smith, D.L., Wyld, S.J., Miller, E.L., and Wright, J.E., 1993, Progression and timing of Mesozoic crustal shortening in the northern Great Basin, western USA, *in* Dunne, G.C., and McDougall, K.A., Mesozoic Paleogeography of the Western United States-II: Los Angeles, California, Pacific Section, Society for Sedimentary Geology (SEPM), p. 389–405.

Smithson, S.B., Brewer, J., Kaufman, S., Oliver, J., and Hurich, C., 1978, Nature of the Wind River thrust, Wyoming, from COCORP deep-reflection data and from gravity data: Geology, v. 6, p. 648–652, https://doi.org/10.1130/0091-7613(1978)6<648:NOTWRT>2.0.CO;2.

Snoke, A.W., and Miller, D.M., 1988, Metamorphic and tectonic history of the northeastern Great Basin, *in* Ernst, W.G., ed., Metamorphism and Crustal Evolution of the Western United States: Englewood Cliffs, New Jersey, Prentice-Hall, Rubey Volume 7, p. 606–648.

Stearns, D.W., 1978, Faulting and forced folding in the Rocky Mountains foreland, *in* Matthews, V., III, ed., Laramide Folding Associated with Basement Block Faulting in the Western United States: Geological Society of America Memoir 151, p. 1–38, https://doi.org/10.1130/MEM151-p1.

Steidtmann, J.R., and Middleton, L.T., 1991, Fault chronology and uplift history of the southern Wind River Range, Wyoming: Implications for Laramide and post-Laramide deformation in the Rocky Mountain foreland: Geological Society of America Bulletin, v. 103, p. 472–485, https://doi.org/10.1130/0016-7606(1991)103<0472:FCAUHO>2.3.CO;2.

Stevens, A.L., Balgord, E.A., and Carrapa, B., 2016, Revised exhumation history of the Wind River Range, WY, and implications for Laramide tectonics: Tectonics, v. 35, p. 1121–1136, https://doi.org/10.1002/2016TC004126.

Strecker, U., 1996, Studies of Cenozoic continental tectonics: Part I. Apatite fission-track thermochronology of the Black Hills uplift, South Dakota. Part II. Seismic sequence stratigraphy of Goshute Valley Halfgraben, Nevada [Ph.D. dissertation]: Laramie, Wyoming, University of Wyoming, 686 p.

Stone, D.S., 1977, Tectonic history of the Uncompahgre Uplift, *in* Veal, H.K., ed., Exploration Frontiers of the Central and Southern Rockies: Rocky Mountain Association of Geologists 1977 Symposium, p. 23–30.

Stone, D.S., and Hollberg, J.E., eds., 1987, Rocky Mountain Transect: The Wyoming Transect: Rocky Mountain Association of Geologists [on CD-ROM].

Tamer, M.T., and Ketcham, R.A., 2020, The along-track etching structure of fission tracks in apatite: Observations and implications: Chemical Geology, v. 553, https://doi.org/10.1016/j.chemgeo.2020.119809.

Tan, Z., Xiao, W., Mao, Q., Wang, H., Sang, M., Li, R., Gao, L., Guo, Y., Gan, J., Liu, Y., and Wan, B., 2022, Final closure of the Paleo Asian Ocean basin in the early Triassic: Communications Earth & Environment, v. 3, 259, https://doi.org/10.1038/s43247-022-00578-4.

Tarduno, J.A., McWilliams, M., Debiche, M.G., Sliter, W.V., and Blake, M.C., 1985, Franciscan Complex Calera limestones: Accreted remnants of Farallon Plate oceanic plateaus: Nature, v. 317, p. 345–347, https://doi.org/10.1038/317345a0.

Taylor, W.J., Bartley, J.M., Martin, M.W., Geissman, J.W., Walker, J.D., Armstrong, P.A., and Fryxell, J.E., 2000, Relations between hinterland and foreland shortening: Sevier orogeny, central North American Cordillera: Tectonics, v. 19, p. 1124–1143, https://doi.org/10.1029/1999TC001141.

ter Voorde, M., de Bruijne, C.H., Cloetingh, S.A.P.L., and Andriessen, P.A.M., 2004, Thermal consequences of thrust faulting: Simultaneous versus successive fault

activation and exhumation: Earth and Planetary Science Letters, v. 223, p. 395–413, https://doi.org/10.1016/j.epsl.2004.04.026.

Thacker, J.O., Kelley, S.A., and Karlstrom, K.E., 2021, Late Cretaceous recent low-temperature cooling history and tectonic analysis of the Zuni Mountains, west-central New Mexico: Tectonics, v. 40, https://doi.org/10.1029/2020TC006643.

Thacker, J.O., Karlstrom, K.E., Kelley, S.A., Crow, R.S., and Kendall, J.J., 2023, Late Cretaceous time-transgressive onset of Laramide arch exhumation and basin subsidence across northern Arizona New Mexico, USA, and the role of a dehydrating Farallon flat slab: Geological Society of America Bulletin, v. 135, p. 389–406, https://doi.org/10.1130/B36245.1.

Tindall, S.E., and Davis, G.H., 1999, Monocline development by oblique-slip fault-propagation folding: The East Kaibab monocline, Colorado Plateau, Utah: Journal of Structural Geology, v. 21, p. 1303–1320, https://doi.org/10.1016/S0191-8141(99)00089-9.

Tindall, S.E., Storm, L.P., Jenesky, T.A., and Simpson, E.L., 2010, Growth faults in the Kaiparowits Basin, Utah, pinpoint initial Laramide deformation in the western Colorado Plateau: Lithosphere, v. 2, p. 221–231, https://doi.org/10.1130/L79.1.

Torsvik, T.H., Steinberger, B., Shephard, G.E., Doubrovine, P.V., Gaina, C., Domeier, M., Conrad, C.P., and Sager, W.W., 2019, Pacific-Panthalassic reconstructions: Overview, errata and the way forward: Geochemistry, Geophysics, Geosystems, v. 20, p. 3659–3689, https://doi.org/10.1029/2019GC008402.

Usui, T., Nakamura, E., Kobayashi, K., Maruyama, S., and Helmstaedt, H., 2003, Fate of the subducted Farallon plate inferred from eclogite xenoliths in the Colorado Plateau: Geology, v. 31, p. 589–592, https://doi.org/10.1130/0091-7613(2003)031<0589:FOTSFP>2.0.CO;2.

Vlaha, D.R., Zuza, A.V., Chen, L., and Harlaux, M., 2024, Hot Cordilleran hinterland promoted lower crust mobility and decoupling of Laramide deformation: Nature Communications, v. 15, 3750, https://doi.org/10.1038/s41467-024-48182-8.

Wagner, G.A., and Van den Haute, P., 1992, Fission-track dating method, *in* Wagner, G.A., and Van den Haute, P., eds., Fission-Track Dating: Springer, p. 59–94, https://doi.org/10.1007/978-94-011-2478-2_3

Weil, A.B., and Yonkee, W.A., 2012, Layer-parallel shortening across the Sevier fold-thrust belt and Laramide foreland of Wyoming: Spatial and temporal evolution of a complex geodynamic system: Earth and Planetary Science Letters, v. 357–358, p. 405–420, https://doi.org/10.1016/j.epsl.2012.09.021.

Weil, A.B., and Yonkee, A., 2023, The Laramide orogeny: Current understanding of the structural style, timing, and spatial distribution of the classic foreland thick-skinned tectonic system, *in* Whitmeyer, S.J., Williams, M.L., Kellett, D.A., and Tikoff, B., eds., Laurentia: Turning Points in the Evolution of a Continent: Geological Society of America Memoir 220, p. 707–723, https://doi.org/10.1130/2022.1220(33).

Weil, A.B., Yonkee, A., and Schultz, M., 2016, Tectonic evolution of a Laramide transverse structural zone: Sweetwater Arch, south central Wyoming: Tectonics, v. 35, p. 1090–1120, https://doi.org/10.1002/2016TC004122.

Wells, M.L., and Hoisch, T.D., 2008, The role of mantle delamination in widespread Late Cretaceous extension and magmatism in the Cordilleran orogen, western United States: Geological Society of America Bulletin, v. 120, p. 515–530, https://doi.org/10.1130/B26006.1.

Wildman, M., Brown, R., Beucher, R., Persano, C., Stuart, F., Gallagher, K., Schwanethal, J., and Carter, A., 2016, The chronology and tectonic style of landscape evolution along the elevated Atlantic continental margin of South Africa resolved by joint apatite fission track and (U-Th-Sm)/He thermochronology: Tectonics, v. 35, p. 511–545, https://doi.org/10.1002/2015TC004042.

Winn, C., Karlstrom, K.E., Shuster, D.L., Kelley, S., and Fox, M., 2017, 6 Ma age of carving westernmost Grand Canyon: Reconciling geologic data with combined AFT, (U-Th)/He, and $^{4}He/^{3}He$ thermochronologic data: Earth and Planetary Science Letters, v. 474, p. 257–271, https://doi.org/10.1016/j.epsl.2017.06.051.

Wright, J.E., and Fahan, M.R., 1988, An expanded view of Jurassic orogenesis in the western United States Cordillera: Middle Jurassic (pre-Nevadan) regional metamorphism and thrust faulting within an active arc environment, Klamath Mountains, California: Geological Society of America Bulletin, v. 100, p. 859–876, https://doi.org/10.1130/0016-7606(1988)100<0859:AEVOJO>2.3.CO;2.

Wyld, S.J., 2002, Structural evolution of a Mesozoic backarc fold-thrust belt in the U.S. Cordillera: New evidence from northern Nevada: Geological Society of America Bulletin, v. 114, p. 1452–1468, https://doi.org/10.1130/0016-7606(2002)114<1452:SEOAMB>2.0.CO;2.

Wyoming State Geological Survey, 2022, Precambrian basement map of Wyoming—Structural configuration: Wyoming State Geological Survey Open File Report 2022-5, 8 p., 1 pl., scale 1:500,000, https://doi.org/10.15786/21183787 (revised 2023).

Yonkee, W.A., and Weil, A.B., 2015, Tectonic evolution of the Sevier and Laramide belts within the North American Cordillera orogenic system: Earth-Science Reviews, v. 150, p. 531–593, https://doi.org/10.1016/j.earscirev.2015.08.001.

Yonkee, W.A., Eleogram, B., Wells, M.L., Stockli, D.F., Kelley, S., and Barber, D.E., 2019, Fault slip and exhumation history of the Willard thrust sheet, Sevier fold-thrust belt, Utah: Relations to wedge propagation, hinterland uplift, and foreland basin sedimentation: Tectonics, v. 38, p. 2850–2893, https://doi.org/10.1029/2018TC005444.

Zehnder, A.T., and Allmendinger, R.W., 2000, Velocity field for the trishear model: Journal of Structural Geology, v. 22, p. 1009–1014, https://doi.org/10.1016/S0191-8141(00)00037-7.

Zuza, A.V., and Cao, W., 2022, Metamorphic core complex dichotomy in the North American Cordillera explained by buoyant upwelling in variably thick crust: GSA Today, v. 33, no. 3-4, p. 4–11, https://doi.org/10.1130/GSATG548A.1.

Zuza, A.V., et al., 2018, Tectonic evolution of the Qilian Shan: An early Paleozoic orogen reactivated in the Cenozoic: Geological Society of America Bulletin, v. 130, p. 881–925, https://doi.org/10.1130/B31721.1.

Zuza, A.V., Jepson, G., and Cao, W., 2025, Reassessing metamorphic core complexes in the North American Cordillera: Earth-Science Reviews, v. 260, https://doi.org/10.1016/j.earscirev.2024.104987.

Science Editor: Wenjiao Xiao
Associate Editor: Timothy Kusky

Manuscript Received 21 February 2024
Revised Manuscript Received 20 November 2024
Manuscript Accepted 6 January 2025